Cancer Biol Med 2025. doi: 10.20892/j.issn.2095-3941.2025.0209

ORIGINAL ARTICLE

A novel biguanide-derivative promotes NEDD4-mediated FGFR1 ubiquitination through BMI1 to overcome osimertinib resistance in NSCLC

Mei Peng[1,2,3], Weifan Wang[2,3], Di Xiao[2,3], Duo Li[2,3], Jun Deng[2,3], Hui Zou[2,3], Xing Feng[2,3], Yunhai Yang[4], Songqing Fan[5], Xiaoping Yang[2,3]

[1]Department of Pharmacy and National Clinical Research Center for Geriatric Disorders, Xiangya Hospital, Central South University, Changsha 410008, China; [2]Department of Oncology, Hunan Provincial People's Hospital, The First Affiliated Hospital of Hunan Normal University, Changsha 410013, China; [3]Key Laboratory of Study and Discovery of Small Targeted Molecules of Hunan Province, Institute of Interdisciplinary Studies, Cancer Institute, School of Pharmaceutical Sciences, Health Science Center, Hunan Normal University, Changsha 410013, China; [4]Department of Oncological Surgery, Shanghai Chest Hospital, Affiliated to Shanghai Jiaotong University School of Medicine, Shanghai 200030, China; [5]Department of Pathology, The Second Xiangya Hospital, Central South University, Changsha 410011, China

ABSTRACT

Objective: Osimertinib (OSI) therapy, a cornerstone in treating non-small cell lung cancer (NSCLC), has been severely limited by rapidly developing acquired resistance. Inhibition of bypass activation using a combination strategy holds promise in overcoming this resistance. Biguanides, with excellent anti-tumor effects, have recently attracted much attention for this potential. The current study investigated whether novel biguanide compounds developed by our team could overcome OSI resistance and the underlying mechanisms were explored.

Methods: A comprehensive screening assay using OSI-resistant cells identified the optimal combination of biguanide compounds with OSI. Proteomics, co-immunoprecipitation mass spectrometry, RNA sequencing, and homologous recombination assays were used to elucidate the molecular mechanisms underlying combination therapy. NSCLC tumor tissues, especially OSI-resistant tissues, obtained from our clinic were used to assess the correlations between key proteins and OSI resistance.

Results: SMK-010, a highly potent biguanide compound, effectively overcame OSI resistance *in vitro* and *in vivo*. Mechanistical studies showed that BMI1/FGFR1 pathway activation is responsible for OSI resistance. Specifically, silencing BMI1 promoted NEDD4-mediated FGFR1 ubiquitination and proteasomal degradation, whereas SMK-010 treatment induced FGFR1 lysosomal degradation. This reduction in FGFR1 levels impaired homologous recombination, increased DNA damage, and surmounted OSI resistance. Analysis of clinical samples revealed overexpression of BMI1 and FGFR1 in NSCLC tissues and represented potential biomarkers for OSI resistance.

Conclusions: These findings highlight the crucial role of the BMI1/FGFR1 axis in OSI resistance and provide a rational basis for the future clinical application of the biguanide, SMK-010, in combination with OSI.

KEYWORDS NSCLC; biguanide; FGFR1 ubiquitination; BMI1; osimertinib resistance

Introduction

Non-small cell lung cancer (NSCLC) constitutes > 85% of all lung cancer malignancies[1], ranking as the second most prevalent cancer globally and demonstrating the highest mortality rate among all cancer types[2]. The development of epidermal growth factor receptor tyrosine kinase inhibitors (EGFR-TKIs) has revolutionized NSCLC treatment by targeting activating EGFR mutations[3,4]. As a pioneering third-generation EGFR-TKI, osimertinib (OSI) has become the first-line treatment for EGFR-mutant NSCLC, as evidenced by its status as

Correspondence to: Yunhai Yang, Songqing Fan and Xiaoping Yang
E-mail: docyyh@163.com, songqingfan@csu.edu.cn and xiaoping.yang@hunnu.edu.cn
ORCID ID: https://orcid.org/0000-0001-9848-3845, https://orcid.org/0000-0002-1486-9909 and https://orcid.org/0000-0003-1952-7227
Received April 24, 2025; accepted July 22, 2025; published online September 10, 2025.
Available at www.cancerbiomed.org

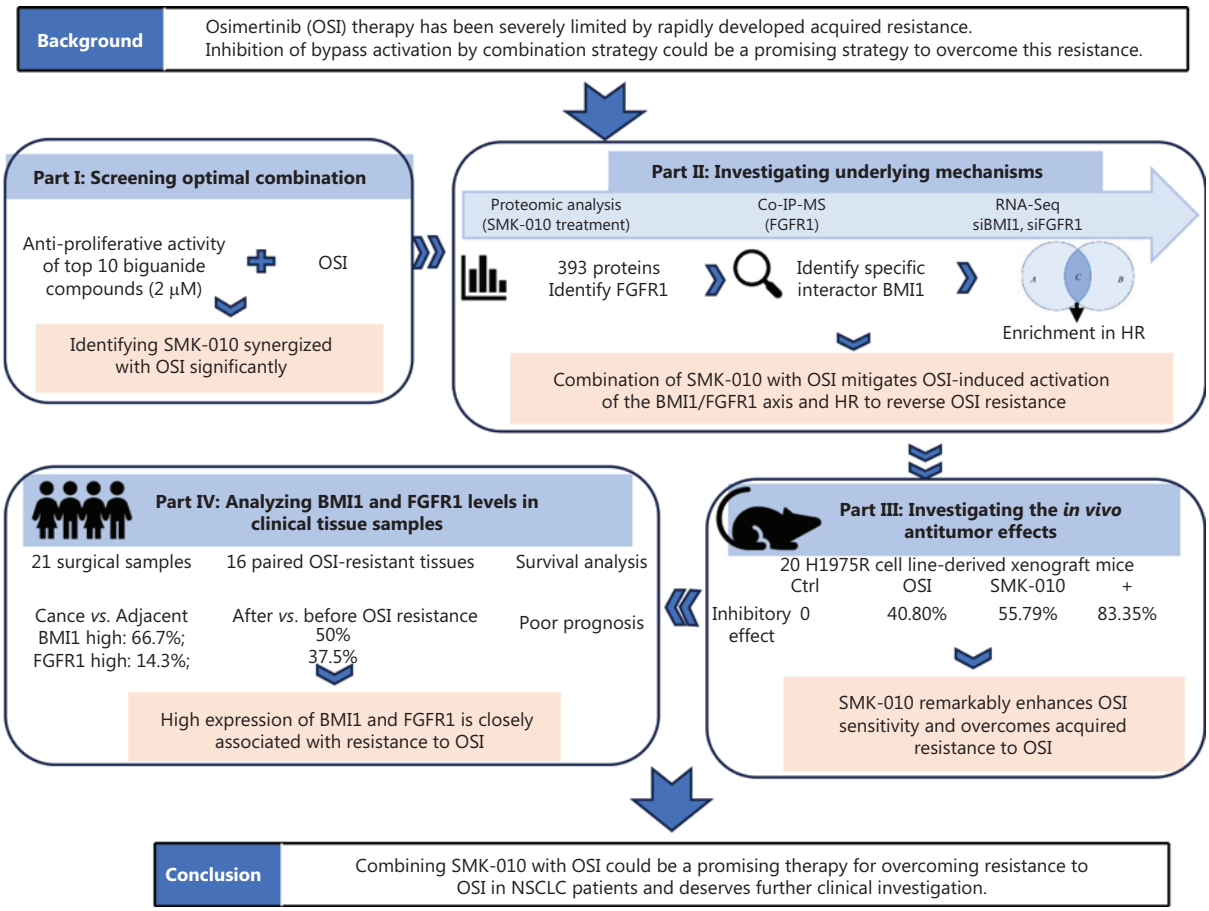

Study flowchart Part I involved a comprehensive screening assay using OSI-resistant cells to identify the optimal combination of biguanide compounds with OSI. Part II outlined the mechanisms underlying the SMK-010 and OSI combination utilizing proteomics, Co-IP-MS, RNA sequencing, and HR assays. Part III examined the *in vivo* anti-tumor effects of combining SMK-010 with OSI using an OSI-resistant cell-derived xenograft model. Part IV analyzed BMI1 and FGFR1 expression in clinical tissue samples, particularly in paired samples from OSI-resistant patients. This study showed that the SMK-010 and OSI combination could represent a promising therapeutic strategy for overcoming OSI resistance in NSCLC patients and warrants further clinical investigation. OSI, osimertinib; Co-IP-MS, co-immunoprecipitation mass spectrometry; HR, homologous recombination.

second highest-grossing drug in the 2023 AstraZeneca financial report[5]. Nevertheless, the emergence of acquired resistance to OSI poses a significant clinical challenge with limited therapeutic options currently available for resistant patients[6-8]. Mechanistically, bypass pathway activation has been identified as a predominant driver of OSI resistance[9,10], suggesting that dual targeting of EGFR-driven oncogenic signaling and compensatory pathways represents a promising therapeutic strategy[11].

FGFR1 tyrosine kinase has important roles in lung carcinogenesis[12,13] with accumulating evidence implicating upregulation in OSI resistance. For example, Terp et al. reported elevated FGFR1 expression and consequent AKT activation in OSI-resistant cell lines[14]. While therapeutic targeting of FGFR signaling has shown promise, clinical translation faces challenges. Specifically, multitarget TKIs have off-target effects[15,16], whereas selective FGFR inhibitors encounter dose-limiting hyperphosphatemia[17]. These limitations highlight the critical need for novel agents capable of effectively suppressing FGFR-mediated resistance with improved safety profiles. The antitumor potential of biguanides has recently attracted great attention. Studies have shown that biguanides enhance the efficacy of chemotherapy or targeted therapy to prevent tumor relapse by targeting tumor heterogeneity. Growing numbers of clinical trials are investigating the antitumor potential of biguanides, such as metformin

and phenformin, primarily in combination treatments[18-21]. However, metformin-based regimens have not achieved clinical approval for cancer therapy, which is potentially attributable to insufficient tumoricidal concentrations following oral administration. Our research team pioneered the rational design of biguanide derivatives through intermediate modification strategies[22]. Most recently, Bridges et al. analyzed the structural basis of biguanide drugs, widening approaches for rational derivative design[23]. Our novel derivatives were shown to have potent antiproliferative effects against wild-type EGFR NSCLC cells[24]. In the current study these compounds also exhibited remarkable anti-proliferative activity in EGFR-mutant NSCLC cells, showing IC_{50} values three orders of magnitude lower than metformin. Systematic screening the combined effects of these derivatives with OSI revealed that SMK-010 synergizes significantly with OSI. Further proteomic profiling identified significant FGFR1 downregulation in SMK-010-treated cells.

In this study SMK-010 was shown to effectively restore OSI sensitivity in resistant models *in vitro* and *in vivo*. How SMK-010 overcame OSI resistance *via* ubiquitinating FGFR1 was elucidated through comprehensive mechanistic studies.

Materials and methods

Cell culture and reagents

H1975P (*L858R/T790M* mutation) and HCC827P (exon 19 deletion) cells, along with their OSI-resistant cells (H1975R and HCC827R), were cultured in RPMI-1640 supplemented with 10% fetal bovine serum (FBS) in a humidified 5% CO_2 incubator at 37°C. H1975P and H1975R cells were generously provided by Professor Yang Shanghai Chest Hospital, Shanghai Jiaotong University School of Medicine, (Shanghai, China). HCC827P and HCC827R cells were kindly provided by Professor Fan The Second Xiangya Hospital, Central South University, (Changsha, Hunan, China). The method for establishing H1975R and HCC827R cells was adopted from a previous report[25]. Briefly, H1975R and HCC827R cell lines were developed from parental H1975 and HCC827 cells by treating the cells with gradient-increasing concentrations of OSI for 72 h with a recovery period between pulses. The initial OSI concentration was equal to the IC_{50} for the respective parental cells after treatment by OSI. Surviving cells were allowed to recover and proliferate to ~80% confluence before the next pulse with OSI concentrations ranging from 0.2–10 μM. The H1975R and HCC827R cell lines were successfully established after 6 months of gradient screening.

All biguanide derivatives were synthesized and structurally verified by nuclear magnetic resonance and LC/MS[26,27]. PTC-209, PD173074, and OSI were purchased from Selleck Chemicals (Houston, TX, USA).

Cell viability assay

Cell viability was determined using the methyl thiazolyl tetrazolium (MTT) assay, as previously described[28]. The combination index (CI) for drug synergism was calculated using CompuSyn software (CompuSyn, Inc. Paramus, NJ, USA).

Clonogenic growth assay

Cells were seeded in 24-well plates at a density of 2.0×10^3 cells per well. The cells were treated with the indicated compounds after 12 h and cultured for 6–8 d. The cells were then washed with PBS, fixed with 4% paraformaldehyde, and stained with 0.1% crystal violet. The colonies were visually examined. Absorbance was measured at 550 nm using a microplate reader (Biotek, Winooski, Vermont, USA). Data were normalized to the control group.

Transwell assay

Tumor cell migration was evaluated using Transwell chambers (Corning, New York, USA). Approximately 4×10^4 cells in 200 μL of serum-free medium were seeded into the upper chambers, while the lower chambers contained 700 μL of medium supplemented with 10% serum as a chemoattractant. Following incubation for 24 h, non-migrated cells on the upper side of the membrane were gently removed with cotton wool. Migrated cells on the lower side of the membrane were fixed with 4% paraformaldehyde, stained with 0.1% crystal violet, and quantified. Five random fields (200× magnification) were counted per chamber and the average values were calculated. Data are presented as the mean ± standard error from three independent experiments.

Western blotting

Protein extracts were separated by SDS-PAGE and transferred onto PVDF membranes. The membranes were then incubated with primary antibodies (**Table S2**), then probed

with peroxidase-conjugated anti-mouse (Signalway Antibody, College Park, Maryland, USA) or anti-rabbit secondary antibodies (Cell Signaling Technology, Danvers, Massachusetts, USA). The antigen-antibody reaction was visualized using a ChemiDoc system (Bio-Rad, Hercules, CA, USA). The band intensities on the blots were quantified using ImageJ software.

Transfection of siRNAs or plasmid

siRNAs, negative control (siCtrl) siRNAs, or human BMI1 gene ORF cDNA clone expression plasmid (RiboBio, Guangzhou, China) were transfected into cells *via* Lipofectamine 6,000 transfection reagent (Invitrogen, Eugene, OR, USA) according to the manufacturer's instructions. The specific silencing or overexpression effect was confirmed by western blot analysis. The sequences of the utilized siRNAs are provided in **Table S3**.

Immunoprecipitation (IP)

Briefly, total proteins were extracted and quantified. A total of 1,000 μg of protein was incubated with 10 μg of anti-BMI1 (Abcam, Cambridge, UK), anti-FGFR1 (Cell Signaling Technology), or anti-IgG antibodies (Cell Signaling Technology) for 12 h at 4°C. Immune complexes were captured using Protein A/G beads (company, Santa Cruz, Dallas, Texas, USA). The beads were washed, eluted in sample buffer, and boiled for 10 min at 100°C. The immune complexes underwent western blot analysis. Anti-IgG was used as a negative control.

RNA isolation and quantitative reverse transcription PCR

RNA was extracted using TRIzol reagent (company, Invitrogen, Eugene, OR, USA). The procedure for subsequent RT-qPCR analysis was performed as described previously[28]. The sequences of primers are listed in **Table S4**.

Immunofluorescence (IF)

Cells were plated on coverslips in 12-well plates and cultured overnight to allow cell adherence. After different treatments cells were fixed with 4% paraformaldehyde, permeabilized with 0.1% Triton X-100, and incubated with primary antibodies overnight at 4°C. The cells were washed with PBS, incubated with DyLight 549- or Alexa Fluor 488-labeled secondary antibodies (Proteintech, Chicago, Illinois, USA) for 60 min at room temperature, and counterstained with DAPI (company, Beyotime, Shanghai, China). Finally, images were captured using an Olympus FV3000 confocal microscope (Olympus, Tokyo, Japan).

Homologous recombination (HR) assay

Cells (3×10^5/well) were transfected with the HR reporter plasmid, pDRGFP (AddGene, Watertown, Massachusetts, USA) in 6-well plates. The following day, cells were transfected with the Sce-I-expressing plasmid (pCBASce-I; AddGene,Watertown, Massachusetts, USA). The cells were treated with SMK-010 and OSI alone or in combination immediately after transfection. The cells were collected and analyzed by flow cytometry 50–60 h post-transfection. Relative HR capacity was calculated as the ratio of the percentage of GFP-positive Sce-I-transfected cells-to-the percentage of basal GFP-positive cells in the mock control.

Cell line-derived xenograft models

All animal studies were pre-approved by the Ethics Committee of Hunan Normal University (D2023004) and performed in accordance with the Guide for the Care and Use of Laboratory Animals. Female BALB/c nude mice (4–6 weeks old weighing 18–20 g) were purchased from Hunan Slack Jingda Experimental Animal Company (Hunan, China). Mice were housed and maintained under specific pathogen-free conditions. Suspensions of H1975R cells (0.2 mL in 50% Matrigel; BD Biosciences, San Jose, California, USA) were injected subcutaneously into the flanks of the mice. When tumors reached an average volume of 100 mm^3, tumor-bearing mice ($n = 5$ per group) were randomly assigned to receive vehicle [OSI (5 mg/kg/day, oral gavage), SMK-010 [6 mg/kg/day, intraperitoneal injection], or OSI + SMK-010. Tumor volume (V = length × $width^2/2$) and body weight were measured every other day. Mice were euthanized when tumor size reached 1,000–1,500 mm^3. Investigators were not blinded to group allocation during the experiment or outcome assessment.

Immunohistochemistry (IHC)

Human tissue samples for this study were obtained from the Second Xiangya Hospital of Central South University

with approval from the Ethics Review Committee (Scientific Research Ethics Committee, No. K021/2021) and informed consent from participating patients. IHC was performed as described previously[28]. BMI1 and FGFR1 staining intensities were scored as 0 (negative), 1 (weak), 2 (medium), or 3 (strong). Staining percentages were graded as follows: 4 (76%–100%); 3 (51%–75%); 2 (26%–50%); 1 (1%–25%); and 0 (0%). Staining score was calculated as the intensity score × percentage score.

RNA-seq

RNA-seq analysis was performed by BGI Co., Ltd. (Shenzhen, China). Briefly, total RNA was extracted using TRIzol reagent and RNA with high purity and integrity was used for RNA-seq. The library was constructed using Optimal Dual-mode mRNA Library Prep Kit (BGI-Shenzhen, China) and sequenced using G400/T7/T10 platform (BGI-Shenzhen, China). The RNA-seq data were aligned with HISAT (2.0.4). The R-DESeq2 package was used to analyze differentially expressed genes (DEGs). Analysis of the RNA-seq data was performed *via* the Dr. Tom System developed by BGI (https://biosys.bgi.com).

IP–MS

IP–MS and analyses were conducted by Genechem Co., Ltd. (Shanghai, China). Briefly, antigen–antibody complexes immobilized on magnetic beads were collected. After enzymatic digestion and peptide desalting, the eluted peptides were collected for liquid chromatography–mass spectrometry analyses using a Q Exactive mass spectrometer (Thermo Fisher Scientific, Waltham, Massachusetts, USA).

Proteomic analysis

H1975R cells were seeded in 75 cm^2 flasks and treated with SMK-010 for 24 h. The cells were then washed twice with PBS and collected. Label-free quantitative proteomics and bioinformatics analyses were performed by Beijing Protein Innovation Co., Ltd. (Beijing, China). Each group was tested in triplicate. R software was used to analyze and plot the data.

Statistical analysis

Statistical analyses were performed using SPSS (version 20.0; IBM, city, IL, USA) and GraphPad Prism 9.0 software (GraphPad, Inc., San Diego, California, USA). Data are presented as the mean ± standard error from three independent experiments. Differences between groups were analyzed using a Student's *t*-test (unpaired for independent groups) or one-way ANOVA followed by Tukey's honestly significant difference (HSD) test, as appropriate based on the homogeneity of variance. A $P < 0.05$ was considered statistically significant.

Results

SMK-010 treatment overcomes OSI resistance

Two pairs of NSCLC parental (H1975P and HCC827P) and OSI-resistant (H1975R and HCC827R) cell lines were selected as experimental models. Drug resistance was confirmed by higher IC_{50} values (> 20-fold) in resistant cells compared to parental cells (H1975P: 0.295 μM *vs.* H1975R: 6.447 μM; HCC827P: 0.212 μM *vs.* HCC827R: 5.315 μM; **Figure 1A**). Clonogenic assays showed that 0.5 μM OSI effectively suppressed parental cell colony formation ($P < 0.001$) but had minimal effect on resistant cells (**Figure 1B, C**). Western blotting revealed decreased E-cadherin and increased N-cadherin and vimentin expression in OSI-resistant cells, indicating the acquisition of epithelial–mesenchymal transition (EMT) characteristics (**Figure 1D**). Furthermore, Transwell assays confirmed significantly increased migratory capacity in OSI-resistant cells compared to parental cells (**Figure 1E**).

The anti-proliferative activities of the top 10 derivatives with OSI were evaluated to identify the optimal combination of OSI with biguanide derivatives (**Table 1**). H1975R cells were treated with OSI ± each compound (2 μM) and cell viability was compared between the combination and monotherapy groups. As shown in **Figure 1G**, SMK-010 emerged as the most potent synergistic agent with OSI (CI values in **Table S1**). Subsequent clonogenic assays demonstrated that 2 μM SMK-010 effectively eradicated OSI-tolerant persisters, reducing colony formation by 74% in H1975R and 58% in HCC827R cells ($P < 0.01$ *vs.* OSI monotherapy; **Figure 1H, I**). Migration assays further revealed synergistic effects of the combination treatments, achieving 84% inhibition compared to 50% with OSI alone ($P < 0.05$; **Figure 1J, K**). Taken together, the findings demonstrated that the combination of SMK-010 and OSI synergistically inhibited NSCLC cell proliferation, colony formation, and migration.

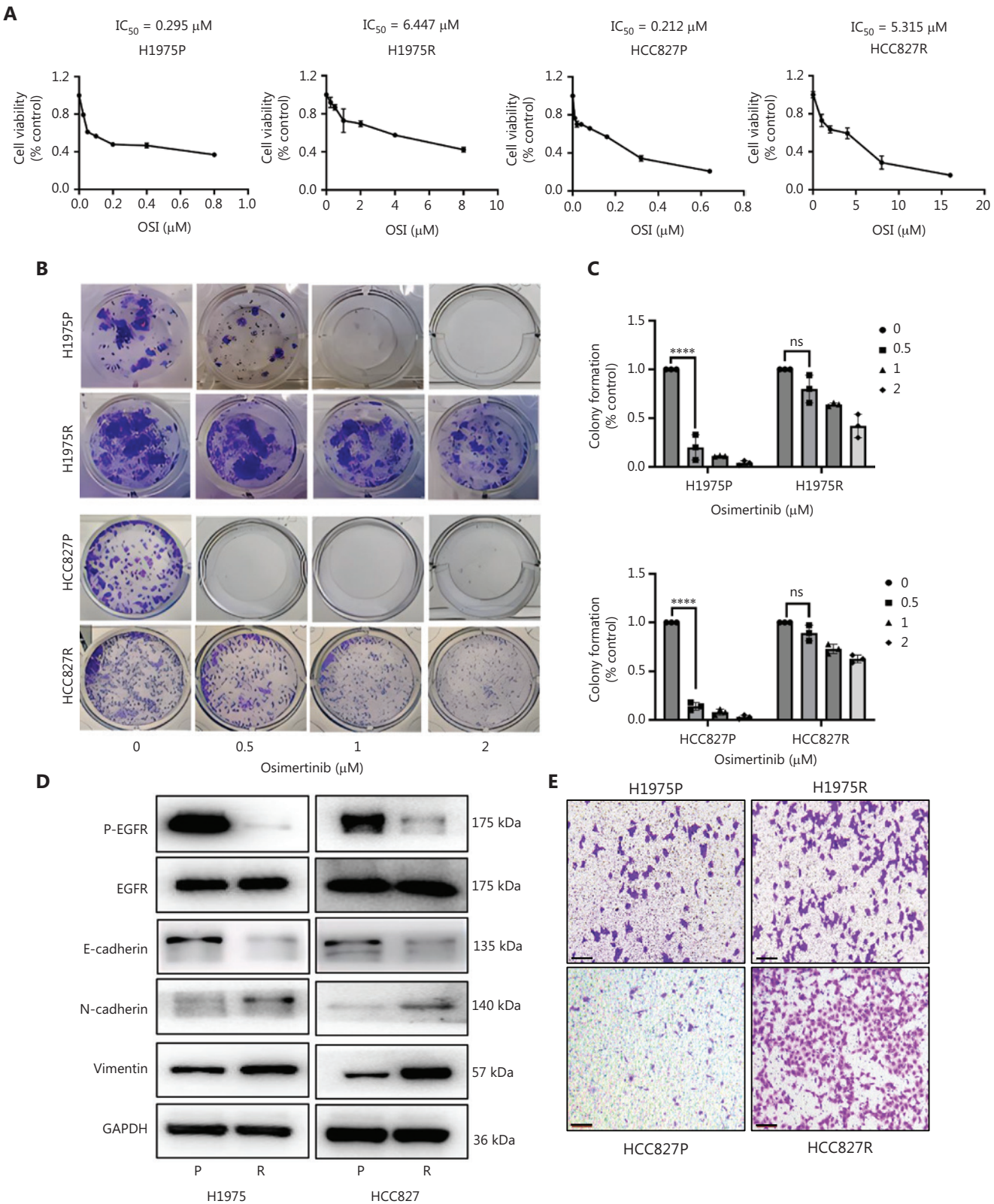

Figure 1 Continued

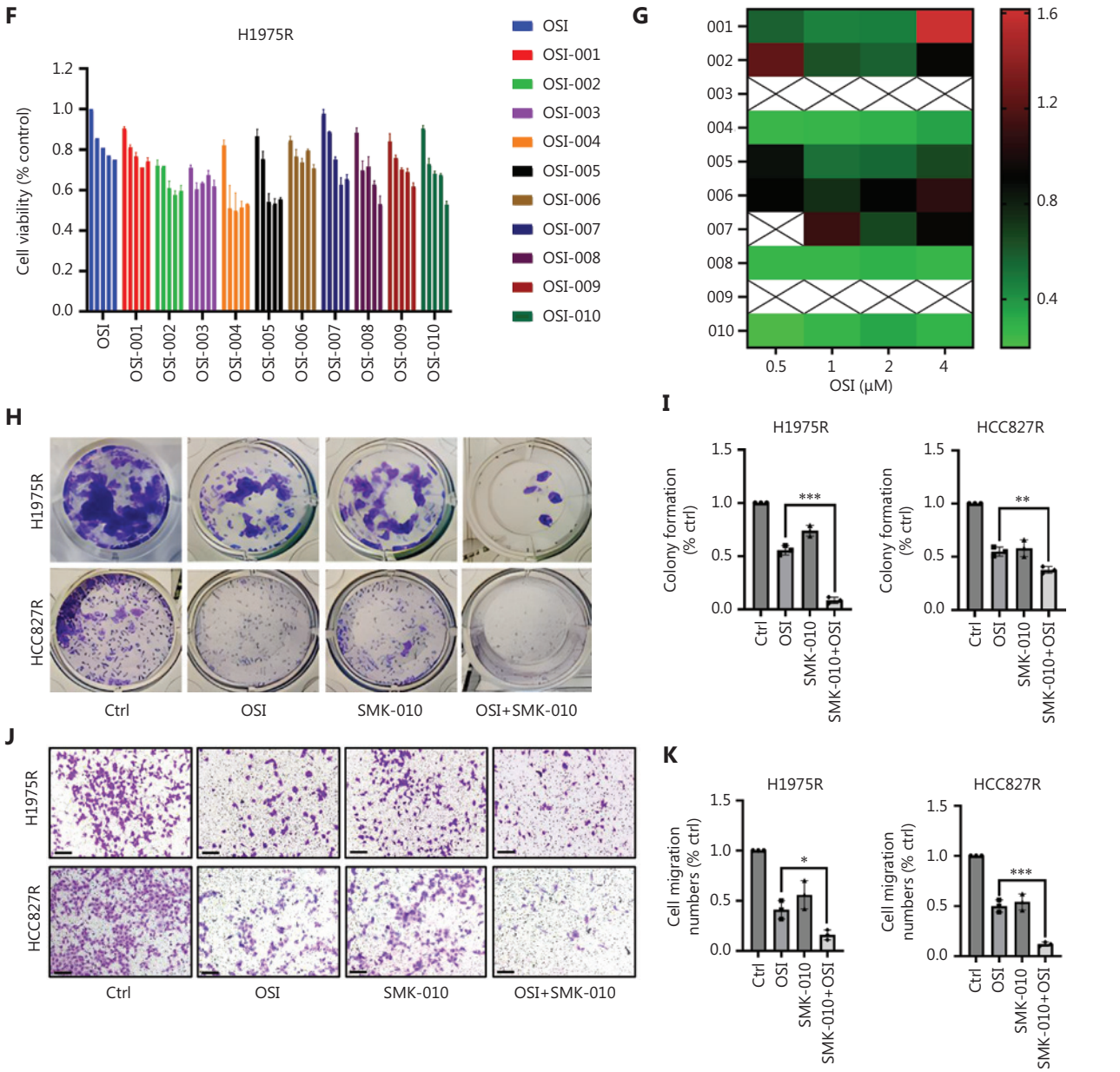

Figure 1 SMK-010 treatment overcomes OSI resistance. (A) The MTT assay determined the IC_{50} of OSI in NSCLC cells (H1975P and HCC827P cells; OSI-resistant H1975R and HCC827R cells). (B, C) Colony formation (B) and quantification (C) analysis of OSI treatment in NSCLC cells. The bars represent the mean ± S.D. of triplicates (****P < 0.0001 for the differences between 0.5 μM OSI and Ctrl in parental cells; ns represents non-significant differences between 0.5 μM OSI and Ctrl in OSI-resistant cells by ANOVA with Tukey's honestly significant difference test for multiple comparisons). (D) Western blot analysis of protein levels in parental and OSI-resistant cells. (E) The Transwell assay detected cell migration in NSCLC cells (scale bar, 25 μm). (F, G) Cell proliferation analysis of the OSI and biguanide derivatives combination in H1975R cells and the calculated combination index (CI). (H, I) Colony formation and quantification analysis of SMK-010 (2 μM), OSI (2 μM) alone, or the combination in OSI-resistant cells. The bars represent the mean ± S.D. of triplicates (***P < 0.001 for the differences between the OSI and OSI + SMK-010 groups in H1975R cells; **P < 0.01 for the differences between the OSI and OSI + SMK-010 groups in HCC827R cells by unpaired t test). (J, K) The Transwell assay (scale bar, 25 μm) and quantification analysis of SMK-010 (2 μM), OSI (2 μM) alone, or combination in OSI-resistant cells. The bars represent the mean ± S.D. of triplicates (*P < 0.05 for the differences between the OSI and OSI + SMK-010 groups in H1975R cells; ***P < 0.001 for the differences between the OSI and OSI + SMK-010 groups in HCC827R cells by unpaired t-test).

Table 1 IC_{50} of metformin and its derivatives in parental and osimertinib-resistant NSCLC cells

Compounds	H1975P (IC_{50} μM)	H1975R (IC_{50} μM)
Metformin	3,479 ± 513	3,057 ± 826
Phenformin	65.893 ± 4.6	22.919 ± 2.8
Proguanil	38.322 ± 1.3	35.756 ± 0.98
SMK-001	7.872 ± 0.91	7.159 ± 1.0
SMK-002	7.613 ± 0.77	6.825 ± 0.54
SMK-003	4.675 ± 0.39	3.100 ± 0.41
SMK-004	6.391 ± 0.90	5.686 ± 0.86
SMK-005	3.032 ± 0.56	2.219 ± 0.43
SMK-006	6.138 ± 0.87	4.946 ± 0.49
SMK-007	4.508 ± 0.74	4.242 ± 0.35
SMK-008	5.030 ± 0.96	3.967 ± 0.66
SMK-009	4.542 ± 0.54	7.722 ± 0.81
SMK-010	4.316 ± 0.39	3.471 ± 0.24

SMK-010 treatment selectively downregulated FGFR1

Proteomic analysis was performed on H1975R cells treated with 6 μM SMK-010 for 24 h to determine the mechanism underlying the synergistic effect between SMK-010 and OSI. We identified 393 differentially expressed proteins (a ratio ≥ 1.2 or ≤ 0.83; $P < 0.05$), including 166 downregulated proteins (**Figure 2A**). Analysis of the top 20 downregulated proteins integrated with RNA-seq data of parental and OSI-resistant cells from GEO datasets showed that the FGFR1 mRNA levels (UniProt ID, P11362) were > 15-fold higher in resistant cells than parental cells. Given the approximately 50% reduction in FGFR1 protein by proteomics, we selected FGFR1 protein for further investigation in resistant cell lines (**Figure 2B, C**). Western blot validation confirmed dose-dependent FGFR1 suppression in both resistant cell lines (H1975R: 49% reduction; HCC827R: 42% reduction; $P < 0.001$; **Figure 2D**). Additionally, the effects of SMK-010 on EGFR, platelet-derived growth factor receptor beta (PDGFRβ), and type 1 insulin-like growth factor receptor (IGF1R) levels were evaluated but no significant changes in the levels of these receptors were detected (**Figure S1A**). Because AKT and extracellular regulated protein kinases 1/2 (ERK1/2) are key downstream effectors of FGFR1, the phosphorylated levels of these proteins were assessed. Consistent with our expectations, exposure to SMK-010 for 24 h reduced the phosphorylation levels of AKT (p-AKT, 42% inhibition) and ERK1/2 (p-ERK1/2, 30% inhibition; $P < 0.01$; **Figure S1B**). These findings provided compelling evidence for the inhibitory effects of SMK-010 on FGFR1 signaling in NSCLC.

OSI treatment increases FGFR1 and BMI1 protein levels

The role of FGFR1 in OSI resistance was investigated. Basal FGFR1 protein levels were significantly higher in OSI-resistant cells than parental cells (**Figure 3A**). Furthermore, OSI treatment (2 μM, 24 h) upregulated FGFR1 by 1.5-fold ($P < 0.01$; **Figure 3B**). FGFR1 is usually located in the cell membrane and cytoplasm. Whether OSI treatment affects the distribution of the FGFR1 protein was also examined. Nuclear–cytoplasmic separation and immunofluorescence results showed that OSI treatment promoted FGFR1 nuclear translocation, increasing nuclear FGFR1 by approximately 80% ($P < 0.001$; **Figure 3C, D**). Co-IP-MS was performed for FGFR1 to determine the proteins that interact with FGFR1 in OSI-resistant cells, which identified BMI1 as a novel FGFR1 interactor (**Figure 3E**, chromatogram shown in **Figure S2**). This interaction was validated by Co-IP and laser confocal microscopy, confirming FGFR1-BMI1 colocalization in the cytoplasm (**Figure 3F, G**). BMI1 has been reported to be an oncoprotein that promotes cancer progression and metastasis[29,30]. However, the role of BMI1 in OSI resistance has not been established. Comparison of the basal levels of BMI1 in parental and OSI-resistant cells revealed significant increases in BMI1 expression in OSI-resistant cells (**Figure 3H**). OSI treatment augmented BMI1expression in a dose-dependent manner (2 μM OSI: 2.0-fold increase; $P < 0.01$; **Figure 3I**). Subcellular analysis showed that OSI increased cytoplasmic (1.3-fold) and nuclear (1.5-fold) BMI1 pools ($P < 0.05$; **Figure 3J**). Confocal immunofluorescence analysis demonstrated OSI treatment enhanced the colocalization of FGFR1 and BMI1 in the cytoplasm and nucleus in resistant cells (**Figure 3K**). However, OSI (4 μM) had a limited effect on p-AKT ($P = 0.16$) and upregulated p-ERK1/2 levels (t = 24 h: Ctrl = 1.30:1, $P < 0.05$) in resistant cells (**Figure S3**). Taken together, these findings suggested that OSI treatment activates BMI1 and FGFR1 and enhances nuclear colocalization, which contribute to resistance in NSCLC.

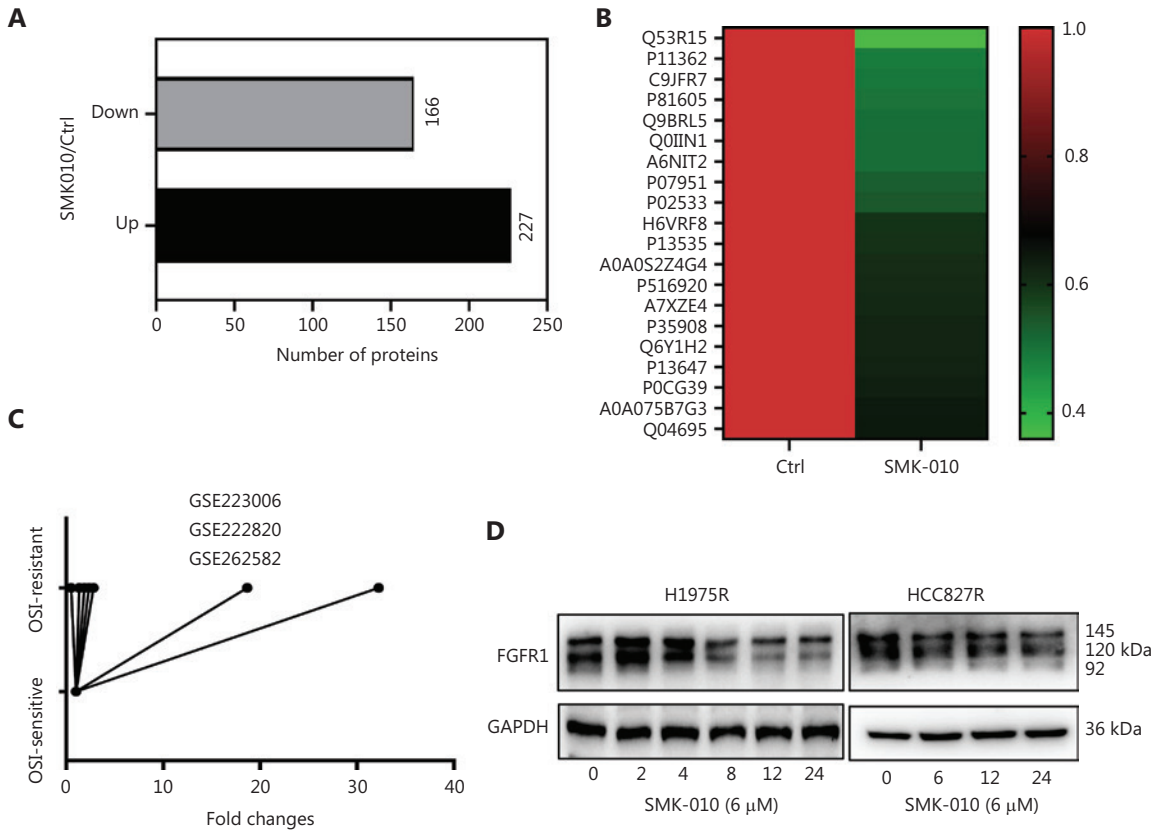

Figure 2 SMK-010 treatment significantly downregulates FGFR1. (A, B) Proteomic analysis of differentially expressed proteins in SMK-010-treated H1975R cells and the top 20 proteins were significantly downregulated. (C) Comparison of mRNA expression (from GEO/RNA-Seq) of the top 20 downregulated proteins in parental *vs.* OSI-resistant cells. (D) Western blot analysis of FGFR1 upon SMK-010 treatment in OSI-resistant cells.

BMI1 stabilizes FGFR1 *via* inhibition of NEDD4-mediated ubiquitination and inhibition of either BMI1 or FGFR1 recovers sensitivity to OSI

Given the consistent OSI-induced changes in BMI1 and FGFR1, the potential regulatory relationship was investigated. BMI1 and FGFR1 were silenced. As shown in **Figure 4A**, silencing BMI1 dramatically reduced the FGFR1 protein level. In contrast, silencing FGFR1 had no effect on BMI1 protein expression, establishing a unidirectional regulatory relationship. Consistently, overexpressing BMI1 increased the FGFR1 protein level (**Figure 4B**). Interestingly, BMI1 knockdown did not downregulate FGFR1 mRNA and FGFR1 knockdown did not affect the BMI1 mRNA level (**Figure 4C**). These findings implied that post-translational modifications are involved in the regulation of FGFR1 by BMI1. BMI1 was depleted in H1975R cells to validate this conclusion and H1975R cells were treated with cycloheximide (CHX), a well-known inhibitor of *de novo* protein synthesis. The FGFR1 protein half-life was subsequently measured. Remarkably, depletion of BMI1 shortened the half-life of FGFRI ($P < 0.05$, **Figure 4D, E**). It is well-known that there are two distinctive protein degradation pathways (the ubiquitin proteasome pathway and the lysosomal proteolysis-mediated pathway)[31]. The commercially available proteasome and lysosomal inhibitors allow a rapid analysis of the possible contributions of each pathway. MG132, a proteasome inhibitor, but not chloroquine (CQ), a lysosomal inhibitor, rescued silencing BMI1-induced FGFR1 downregulation (**Figure 4F**). This finding suggested that after silencing BMI1, FGFR1 undergoes degradation in a ubiquitin–proteasome-dependent manner.

How BMI1 stabilizes the FGFR1 protein was investigated. The E3 ubiquitin ligases, CBL and NEDD4, are reported to

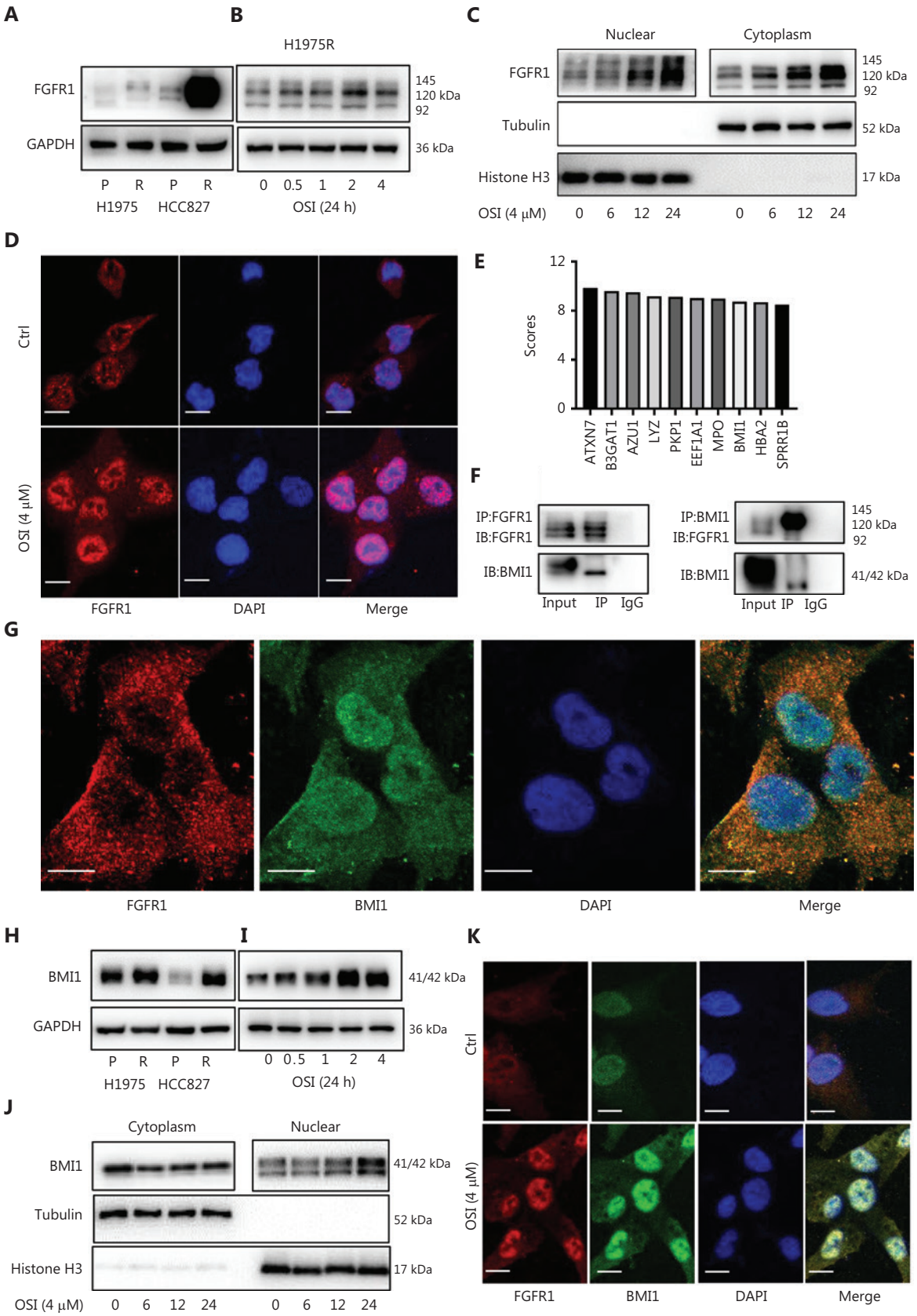

Figure 3 Continued

Figure 3 OSI treatment increases levels of FGFR1 and BMI1 protein. (A) Western blot analysis of FGFR1 in parental and OSI-resistant cells. (B) Western blot analysis of FGFR1 expression upon OSI treatment. (C) Nuclear-plasmic separation and Western blot analysis of FGFR1 in the nucleus and cytoplasm upon OSI treatment. (D) Immunofluorescence (IF) detection of FGFR1 expression and localization upon OSI treatment (scale bar, 15 μm). (E) Immunoprecipitation mass spectrometry (IP-MS) analysis of FGFR1-interacting proteins in H1975R cells. (F) Co-IP and western blot analysis of the binding between FGFR1 and BMI1. (G) IF detection of BMI1 and FGFR1 localization (scale bar, 15 μm). (H) Western blot analysis of BMI1 expression in parental and OSI-resistant cells. (I) Western blot analysis of BMI1 expression upon OSI treatment. (J) Nuclear-plasmic separation and western blot analysis of BMI1 in the nucleus and cytoplasm upon OSI treatment. (K) IF detection of BMI1 and FGFR1 expression and localizations upon OSI treatment (scale bar, 15 μm).

be involved in regulating the stability of the FGFR1 protein. CBL has been shown to play a role in FGFR1 ubiquitination through binding to FRS2 *via* Grb2[32]. NEDD4 belongs to the HECT-type E3 ubiquitin ligase family and is responsible for recognizing specific substrates and mediating ubiquitination. NEDD4 was reported to bind directly to and ubiquitylate FGFR1. These findings led to investigating if CBL or NEDD4 was involved in silencing BMI1-induced FGFR1 degradation. Therefore, CBL and NEDD4 were knocked down using siRNA. Then, the effects of silencing CBL or NEDD4 on silencing BMI1-induced FGFR1 downregulation were determined[33,34]. As shown in **Figure 4G and H**, silencing NEDD4 rescued FGFR1 downregulation induced by BMI1 depletion, whereas CBL depletion had no effect on the FGFR1 protein level (**Figure S4**). Furthermore, co-IP assays demonstrated that NEDD4 silencing significantly inhibited BMI1 depletion-induced FGFR1 ubiquitination (**Figure 4I**). Taken together, these results suggested that NEDD4 is required for depletion of BMI1 to mediate FGFR1 proteasome degradation.

Given the BMI1-FGFR1 regulatory hierarchy, pharmacologic targeting of this axis was determined in OSI-resistant NSCLC models. BMI1 suppression *via* siRNA enhanced OSI sensitivity (**Figure 4J**). Pharmacologic inhibition with PTC-209 (a BMI1 specific inhibitor) demonstrated single-agent activity (28% growth inhibition at 1 μM) and synergistic effects when combined with OSI (CI < 0.65 in H1975R cells, **Figure 4K–M**; CI < 0.8 in HCC827R cells, **Figure 4N**). Clonogenic assays confirmed these findings, showing 56%–75% reduction in resistant cell colony formation with combination treatment (**Figure 4N, O**). Parallel studies targeting FGFR1 yielded complementary results. Silencing FGFR1 enhanced OSI efficacy (**Figure 4P**) and co-treatment with the FGFR1 inhibitor, PD173074, achieved synergistic growth inhibition in both resistant cell models (CI < 0.8, **Figure 4Q–S**). This combination effectively suppressed colony formation by 56%–79% across resistant models (**Figure 4T, U**). These data suggested that inhibiting the BMI1 or FGFR1 signaling pathway may be an effective strategy to increase the antitumor activity of OSI in resistant cells.

SMK-010 treatment inhibits BMI1 and accelerates FGFR1 lysosomal degradation

Because SMK-010 inhibits FGFR1 signaling, the effect on BMI1 was further investigated. Western blot analysis showed that 24 h of treatment with 6 μM SMK-010 downregulated BMI1 (**Figure 5A**). RT-qPCR results revealed that the FGFR1 transcript level was not affected by SMK-010 (**Figure 5B**), suggesting that SMK-010 modulates the post-translational modification of FGFR1 protein. Next, how SMK-010 triggers the degradation of FGFR1 was determined. As shown in **Figure 5C and D**, SMK-010 shortened the half-life of FGFR1. Interestingly, CQ rescued SMK-010-induced FGFR1 downregulation unlike MG132, suggesting that FGFR1 is degraded in lysosomes upon SMK-010 treatment (**Figure 5E, F**). Finally, whether FGFR1 degradation is mediated by ubiquitinases was determined. A comparison of the effects of silencing NEDD4 or CBL on FGFR1 downregulation induced by SMK-010 treatment revealed that silencing NEDD4 weakened FGFR1 downregulation induced by SMK-010 treatment, whereas silencing CBL had no significant effect on this process (**Figure 5G, H**). Together with the results of the FGFR1 Co-IP and ubiquitination assays (**Figure 5I**), SMK-010 was shown to inhibit BMI1 and promote FGFR1 degradation *via* lysosomal pathways. Whether SMK-010 treatment promoted FGFR1 degradation after inhibition of BMI1 was determined. Interestingly, silencing BMI1 weakened the decrease in FGFR1 expression induced by SMK-010 treatment (**Figure 5J, K**), suggesting that SMK-010 promotes the ubiquitination of FGFR1 through BMI1.

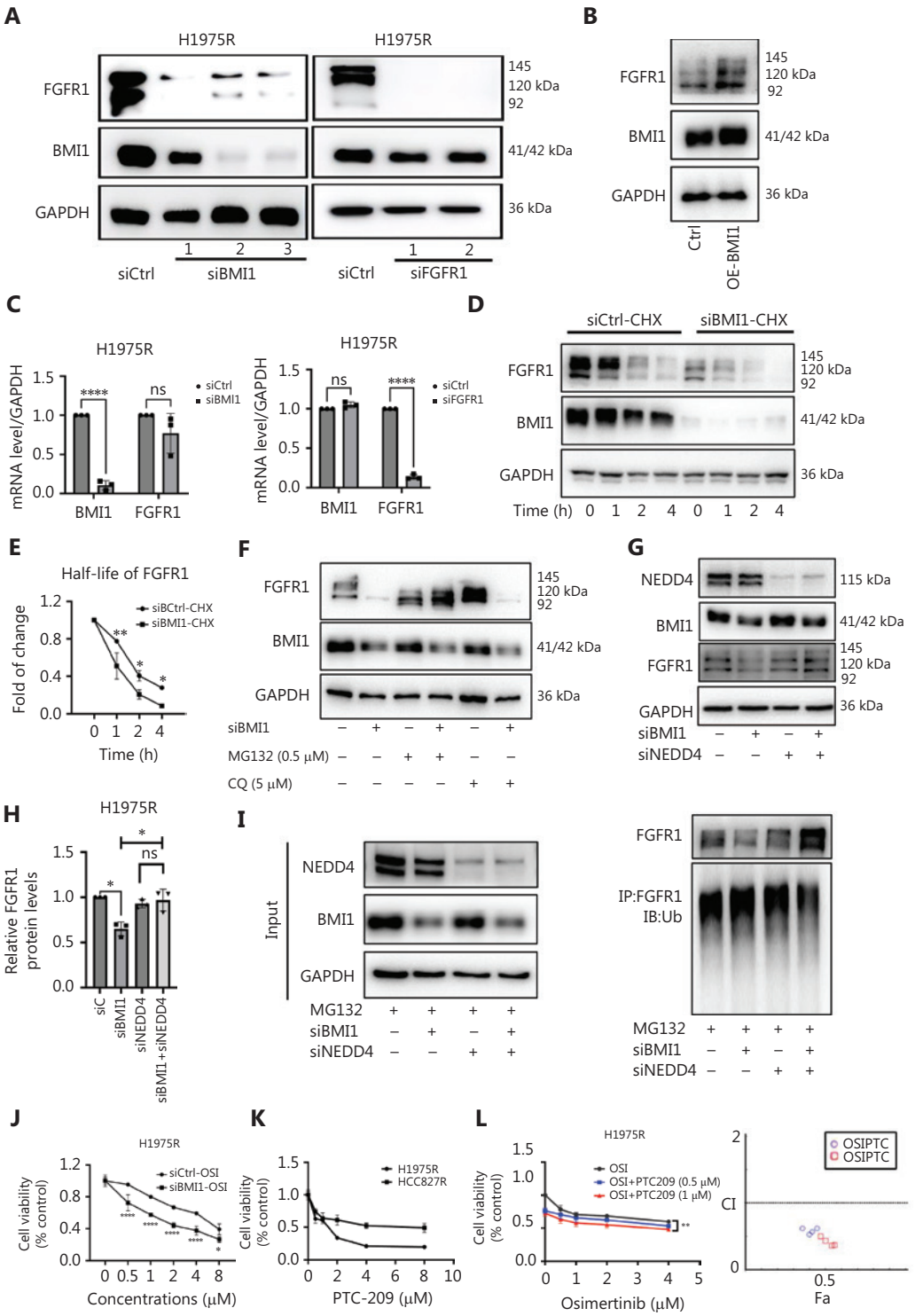

Figure 4 Continued

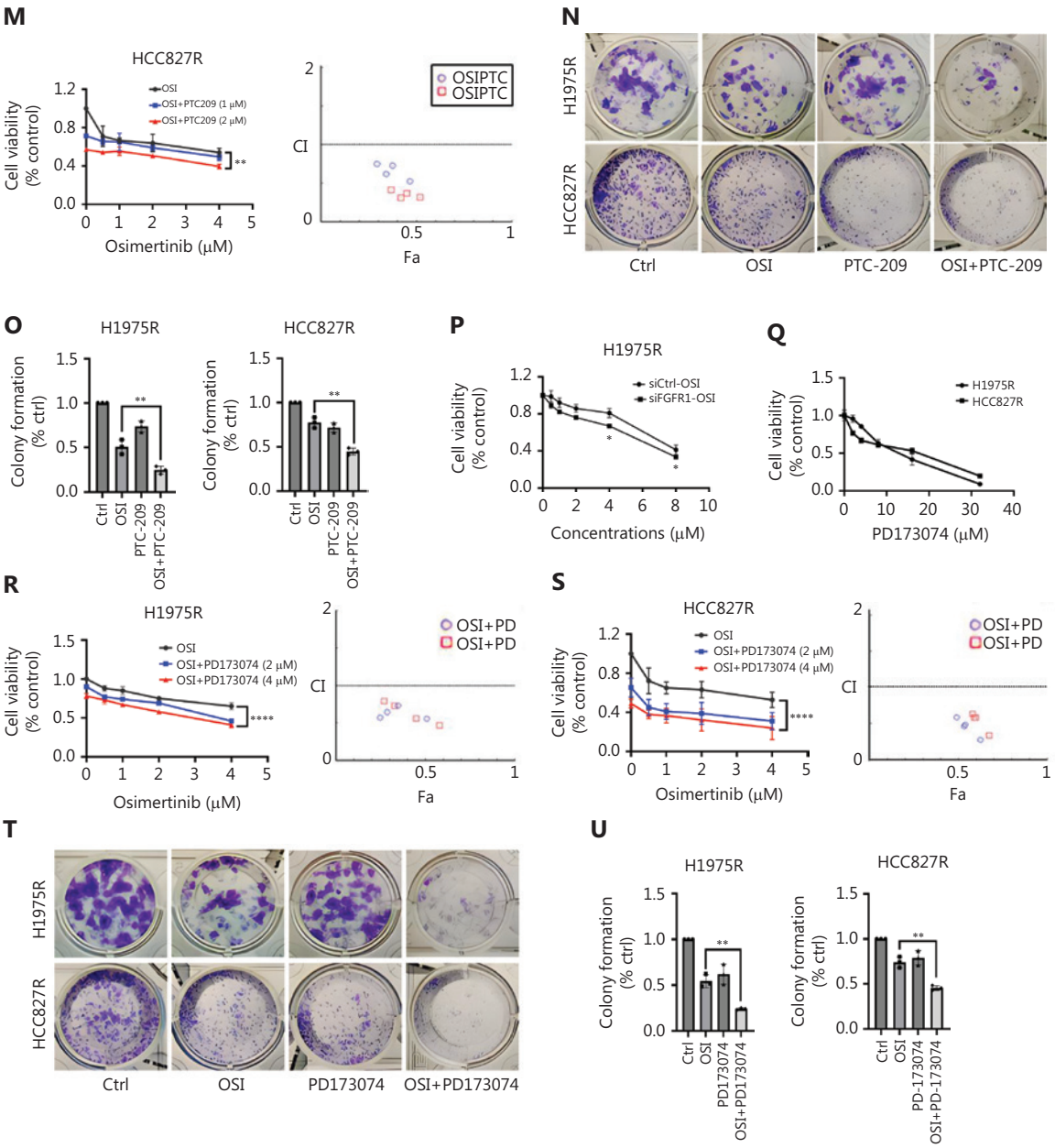

Figure 4 BMI1 stabilizes FGFR1 *via* inhibition of NEDD4-mediated ubiquitination and inhibition of BMI1 or FGFR1 recovers sensitivity to OSI. (A) Western blot analysis of BMI1 and FGFR1 upon silencing BMI1 or FGFR1. (B) Western blot analysis of BMI1 and FGFR1 upon overexpression of BMI1. (C) RT-qPCR analysis of BMI1 and FGFR1 mRNA levels upon silencing BMI1 or FGFR1. The bars represent the mean ± S.D. of triplicates (****P < 0.0001 for the differences in the BMI1 mRNA level between the siCtrl and siBMI1 groups and in the FGFR1 mRNA level between the siCtrl and siFGFR1 groups; ns represents non-significant differences in the FGFR1 mRNA level between the siCtrl and siBMI1 groups and in the BMI1 mRNA level between the siCtrl and siFGFR1 groups, as determined by ANOVA with Tukey's honestly significant difference test for multiple comparisons). (D, E) Western blot (D) and quantification (E) analysis of silencing BMI1 on the FGFR1 half-life. The bars represent the mean ± S.D. of triplicates (**P < 0.01 for the difference between siCtrl at 1 h; *P < 0.05 for the difference between siCtrl at 2 and 4 h determined by ANOVA with Tukey's honestly significant difference test for multiple comparisons). (F) Western blot analysis of MG132 and CQ effects on silencing the BMI1-mediated FGFR1 decrease. (G-I) Western blot and quantification analysis of silencing NEDD4 effect on silencing BMI1-mediated FGFR1 ubiquitin degradation. The bars represent the mean ± S.D. of triplicates (*P < 0.05 for the differences in FGFR1 expression between the siCtrl and siBMI1 groups and between the siBMI1 and siBMI1 + siNEDD4 groups; ns represents non-significant differences in FGFR1 expression between the siNEDD4 and siBMI1 + siNEDD4 groups as determined by an unpaired t-test). (J) The MTT assay detected

the effect of silencing BMI1 on sensitivity to OSI. The bars represent the mean ± S.D. of triplicates (****P < 0.0001 and *P < 0.05 for the differences between siBMI1-OSI and siCtrl-OSI groups by ANOVA with Tukey's honestly significant difference test for multiple comparisons). (K) The MTT assay detected cell proliferation upon PTC-209 treatment. (L) Cell proliferation analysis of the OSI and PTC-209 combination in H1975R cells and the calculated CI. The bars represent the mean ± S.D. of triplicates [**P < 0.01 for the differences between the OSI and OSI + PTC (1 μM) groups by an unpaired *t*-test]. (M) Cell proliferation analysis of the OSI and PTC-209 combination in HCC827R cells and the calculated CI. The bars represent the mean ± S.D. of triplicates [**P < 0.01 for the differences between the OSI and OSI + PTC (2 μM) groups by an unpaired *t*-test]. (N, O) Colony formation (O) and quantification (P) analysis of OSI (2 μM), PTC-209 (1 μM) alone, or the combination in OSI-resistant cells. The bars represent the mean ± S.D. of triplicates (**P < 0.01 for the differences between the OSI and OSI + PTC-209 groups by an unpaired *t*-test). (P) The MTT assay detected the effect of silencing FGFR1 on sensitivity to OSI. The bars represent the mean ± S.D. of triplicates (*P < 0.05 for the differences between the siFGFR1-OSI and siCtrl-OSI groups by ANOVA with Tukey's honestly significant difference test for multiple comparisons). (Q) MTT assay detected the cell proliferation upon PD173074 treatment. (R) Cell proliferation analysis of the OSI and PD173074 combination in H1975R cells and the calculated CI. The bars represent the mean ± S.D. of triplicates [****P < 0.0001 for the differences between the OSI and OSI + PD173074 (4 μM) groups by an unpaired *t*-test]. (S) Cell proliferation analysis of the OSI and PD173074 combination in HCC827R cells and the calculated CI. The bars represent the mean ± S.D. of triplicates [****P < 0.0001 for the differences between the OSI and OSI + PD173074 (4 μM) groups by an unpaired *t*-test]. (T, U) Colony formation (T) and quantification (U) analysis of OSI (2 μM), PD173074 (2 μM) alone, or the combination in OSI-resistant cells. The bars represent the mean ± S.D. of triplicates (**P < 0.01 for the differences between the OSI and OSI + PD173074 groups by an unpaired *t*-test).

SMK-010 treatment attenuates OSI-induced upregulation of BMI1 and FGFR1 to inhibit HR

The synergistic effect of combining OSI with SMK-010 was attributed to sustained inhibition of the FGFR1 pathway. As shown in **Figure 6A and B**, SMK-010 treatment effectively reduced the OSI-induced increase in BMI1 and FGFR1 protein levels.

RNA-seq analysis was performed after BMI1 or FGFR1 knockdown in resistant cells to better understand the functions of BMI1 in OSI resistance in NSCLC. Upregulation of 1,559 genes occurred, whereas 1,475 genes were downregulated by knockdown of BMI1 (**Figure S5A**), suggesting that BMI1 functions as a transcriptional activator along with the well-known transcriptional repression role in cancer. While 42.4% of the FGFR1-regulated genes were also regulated by BMI1, only 28.4% of the BMI1-regulated genes overlapped with FGFR1 regulation (**Figures 6C and S5B**), suggesting an independent role for BMI1 in addition to regulating FGFR1. KEGG pathway analysis of BMI1 knockdown DEGs revealed enrichment in the cell cycle, microRNAs in cancer, pathways in cancer, focal adhesion, and DNA replication. Additionally, classic signaling pathways involved in cancer development, such as the Hippo, Notch, and MAPK signaling pathways, were also enriched (**Figure 6D**). FGFR1 knockdown DEGs were enriched in DNA replication, cell cycle regulation, the Fanconi anemia pathway, pathways associated with cancer, and HR. Furthermore, the FGFR-PI3K-Akt and MAPK downstream signaling pathways were also enriched (**Figure 6E**). KEGG pathway analysis of commonly DEGs upon BMI1 or FGFR1 knockdown revealed enrichment in DNA damage repair pathways, including HR, mismatch repair, and base excision repair (**Figure 6F**). Knocking down BMI1 or FGFR1 significantly downregulated 11 HR-related genes (**Figure 6G**). RT-qPCR validation confirmed decreased mRNA levels of five representative HR-related genes (*RAD51*, *RAD54L*, *XRCC2*, *XRCC3*, and *BLM*) upon BMI1 or FGFR1 knockdown in H1975R cells (**Figure 6H**). Collectively, these RNA-seq analyses strongly suggested that BMI1 or FGFR1 knockdown impaired homologous recombination repair (HRR).

Next, the effects of SMK-010 and OSI on HR in resistant cells were investigated. As shown in **Figure 6I**, treatment with 4 μM OSI alone increased HR activity, whereas treatment with 6 μM SMK-010 alone suppressed HR activity. Notably, the combination of SMK-010 with OSI restored HR to baseline levels. To assess DNA damage status, p-H_2AX expression was evaluated using immunofluorescence. As shown in **Figure 6J**, OSI alone increased p-H_2AX expression and this increase was augmented when OSI was combined with SMK-010. These findings suggested that SMK-010 enhances DNA damage by decreasing HR, thereby overcoming resistance to OSI.

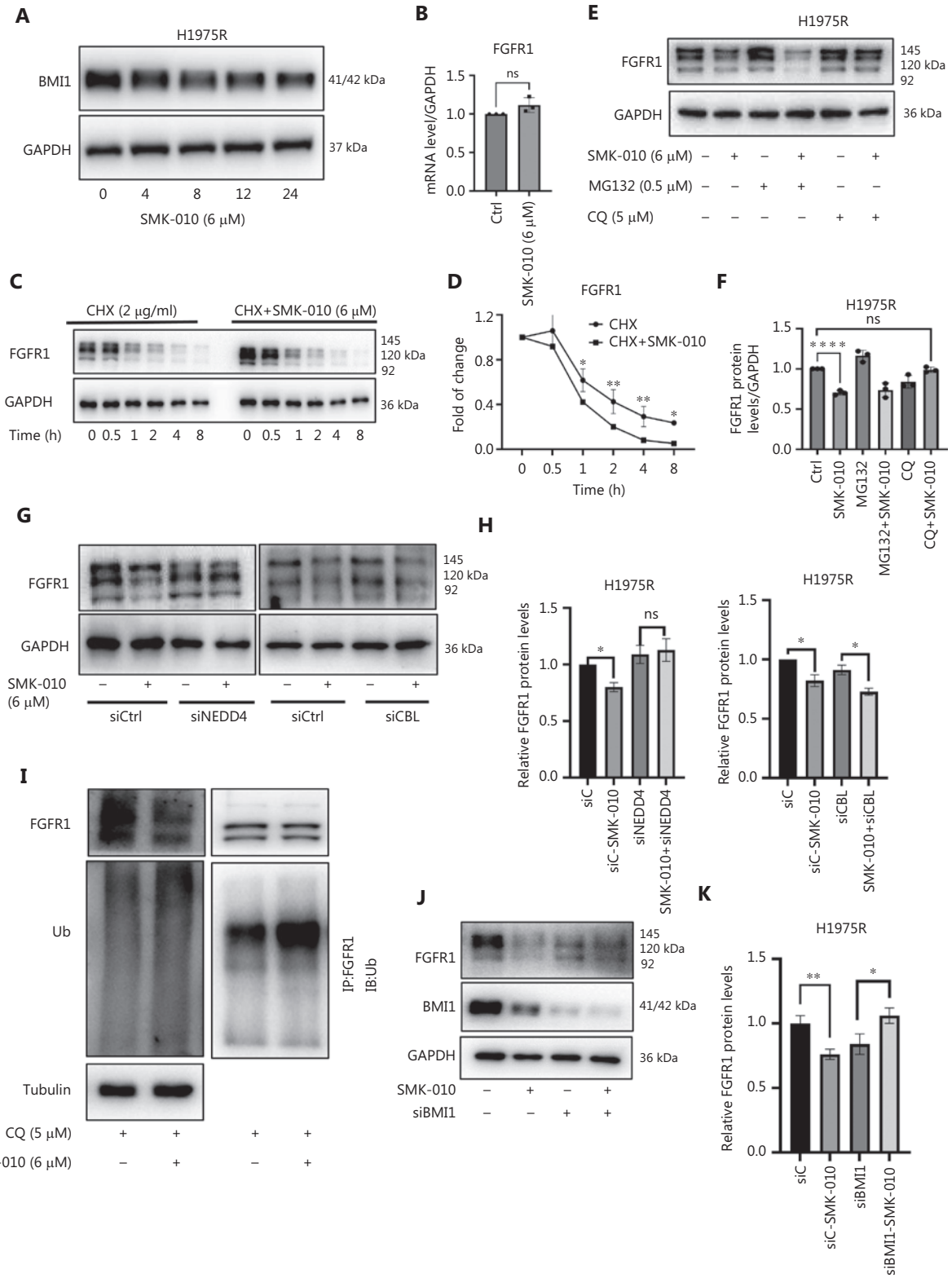

Figure 5 Continued

Figure 5 SMK-010 treatment inhibits BMI1 and accelerates FGFR1 lysosomal degradation. (A) Western blot analysis of BMI1 expression upon SMK-010 treatment. (B) RT-qPCR analysis of FGFR1 mRNA levels upon SMK-010 treatment. The bars represent the mean ± S.D. of triplicates (ns represents non-significant differences between the Ctrl and SMK-010 groups by an unpaired *t*-test). (C, D) Western blot (C) and quantification (D) analyses of SMK-010 on the FGFR1 half-life. The bars represent the mean ± S.D. of triplicates (*P < 0.05 and **P < 0.01 for the differences between the CHX and CHX + SMK-010 groups as determined by ANOVA with Tukey's honestly significant difference test for multiple comparisons). (E, F) Western blot and quantification analyses of MG132 and CQ effects on the SMK-010-mediated FGFR1 decrease. The bars represent the mean ± S.D. of triplicates (****P < 0.0001 for the differences in FGFR1 expression between the Ctrl and SMK-010 groups; ns represents non-significant differences in FGFR1 expression between the Ctrl and CQ + SMK-010 groups by an unpaired *t*-test). (G, H) Western blot and quantification analyses of silencing NEDD4 or CBL effect on the SMK-010-mediated FGFR1 decrease. The bars represent the mean ± S.D. of triplicates (*P < 0.05 for the differences in FGFR1 expression between the siCtrl and siCtrl-SMK-010 groups and between the siCBL and SMK-010 + siCBL groups; ns represents non-significant differences in FGFR1 expression between the siNEDD4 and siNEDD4 + SMK-010 groups by an unpaired *t*-test). (I) Co-IP and western blot analysis of FGFR1 ubiquitin degradation upon SMK-010 treatment. (J, K) Western blot and quantification analyses of effect of silencing BMI1 on the SMK-010-mediated FGFR1 decrease. The bars represent the mean ± S.D. of triplicates (**P < 0.01 for the differences in FGFR1 expression between the siCtrl and siCtrl-SMK-010 groups; *P < 0.05 for the differences in FGFR1 expression between the siBMI1 and siBMI1-SMK-010 groups by an unpaired *t*-test).

SMK-010 treatment effectively impedes OSI resistance *in vivo*

Finally, the antitumor effects of SMK-010 and OSI were assessed using an H1975R cell line-derived xenograft model. Mice were treated daily with vehicle, OSI, SMK-010, or OSI + SMK-010 from day 14–29. OSI alone had limited effects on suppressing tumor growth with an inhibition rate of approximately 40%. In contrast, SMK-010 alone potently inhibited tumor growth with an inhibition rate up to 55%. The combination of OSI and SMK-010 strongly suppressed H1975R tumor growth with an inhibition rate exceeding 80% (**Figure 7A, B**). These findings were consistent with tumor weight assessment (**Figure S6A**). No significant adverse events, including weight loss, were observed during these treatments (**Figure S6B**). Hematoxylin and eosin (HE) staining with glutamic pyruvic transaminase (ALT) and glutamic oxaloacetic transaminase (AST) assays (H1975R: normal *vs.* OSI + SMK-010, $P = 0.1258$; **Figure 7C, D**) further confirmed that SMK-010 alone or SMK-010 combined with OSI did not induce noticeable liver or kidney toxicity in nude mice. Finally, western blot analysis of tumors revealed that the combination of SMK-010 and OSI weakened OSI-induced increases in BMI1 and FGFR1 *in vivo* (**Figure 7E**).

These data suggested that SMK-010 significantly enhances OSI sensitivity and overcomes acquired resistance to OSI, which provides a strong rationale for exploring this combination in the clinic in the future.

High BMI1 and FGFR1 expression are correlated with poor prognosis and OSI resistance in NSCLC patient tissues

To explore the clinical significance of BMI1 expression in NSCLC, 21 surgical samples from NSCLC patients were analyzed. Compared to adjacent tissues, BMI1 was highly expressed in cancer tissues from 14 patients (66.7%). **Figure 8A and B** show representative IHC and western blot results, respectively, for samples with high BMI1 expression in cancer tissues. **Figure 8C** shows that BMI1 was significantly higher in cancer tissues ($P = 0.0092$). Next, the relationship between BMI1 expression and the prognosis of NSCLC patients in the public database was evaluated. As shown in **Figure 8D**, Kaplan-Meier analysis revealed that high BMI1 expression was correlated with shorter overall survival among NSCLC patients.

Next, the correlation between BMI1 expression and OSI resistance was determined in 16 paired EGFR-mutated NSCLC tissues before and after relapse. The results revealed that BMI1 levels were elevated in one-half of the resistant cases [8/16 (50%)], decreased in a minority of the resistant cases [1/16 (6.25%)], and remained unchanged in the remaining resistant cases [7/16 (43.75%)] compared to corresponding baseline counterpart tissues (**Figure 8E**). **Figure 8F** shows IHC images of three representative OSI-resistant lung tissues stained with BMI1 before and after treatment. Quantitative analysis of the IHC results revealed that BMI1 levels were significantly elevated in OSI-resistant patients ($P = 0.0397$; **Figure 8G**). Taken

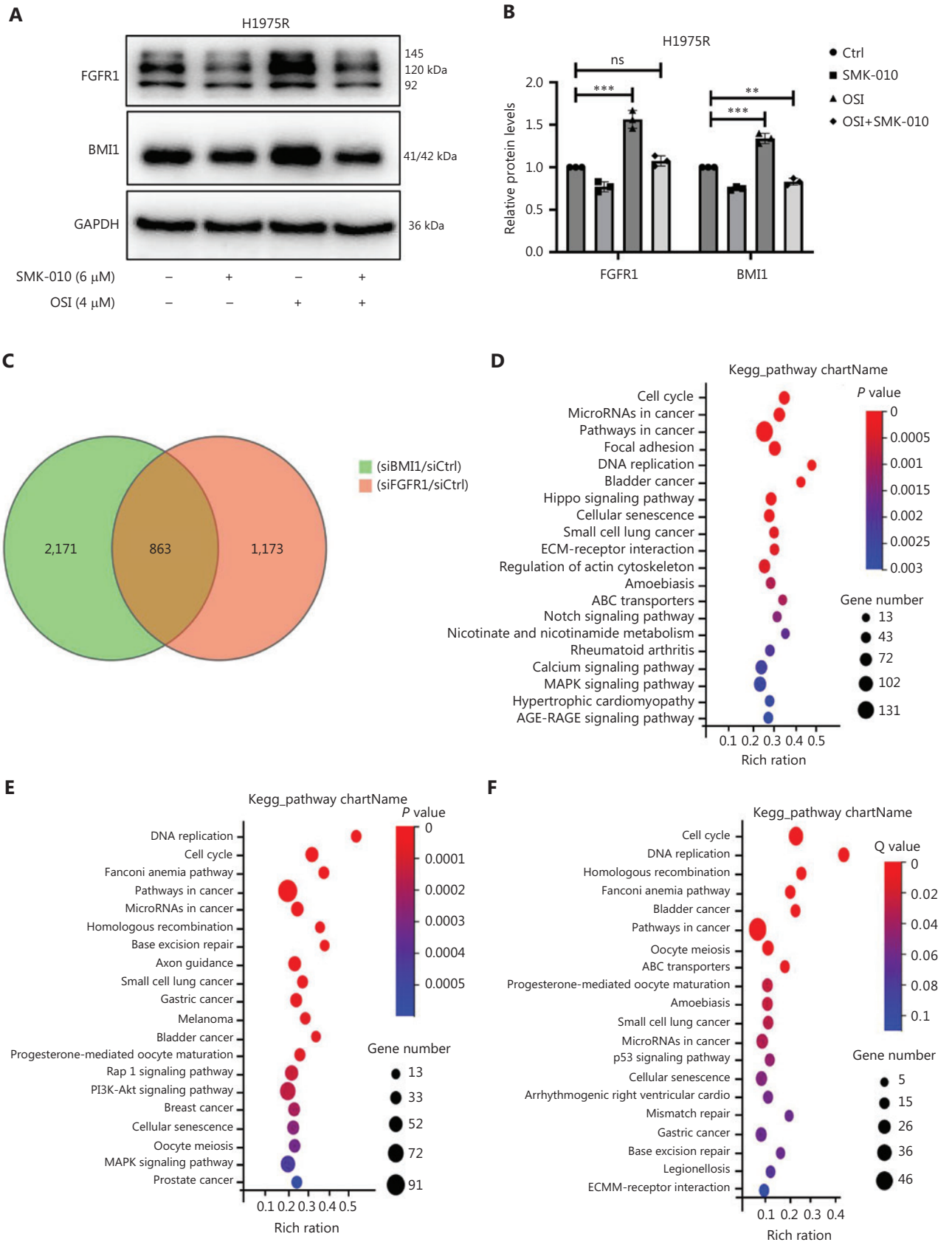

Figure 6 Continued

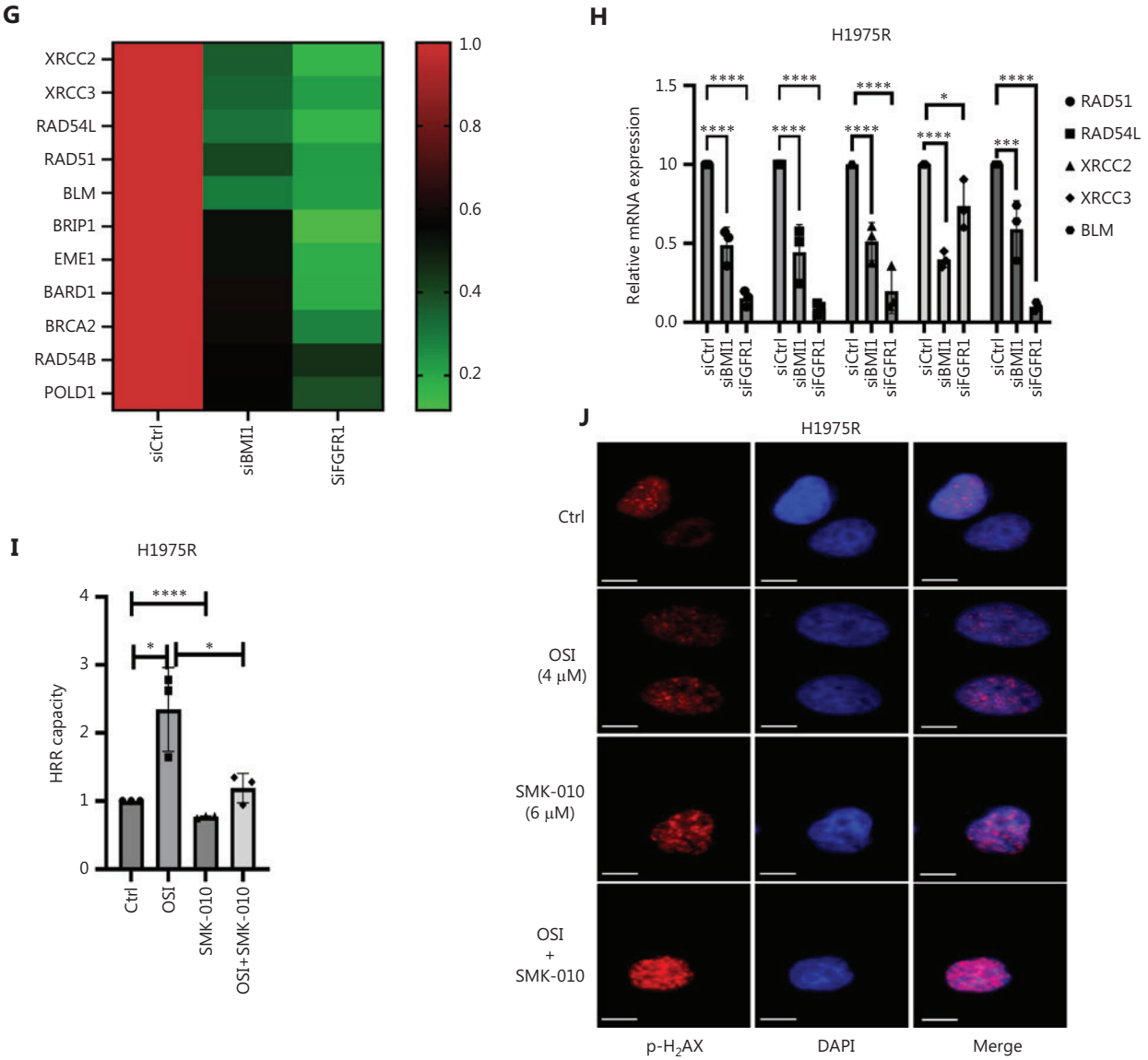

Figure 6 SMK-010 treatment attenuates OSI-induced upregulation of BMI1 and FGFR1 to inhibit HR. (A, B) Western blot and quantification analyses of BMI1 and FGFR1 expression upon SMK-010 and OSI combination treatment. The bars represent the mean ± S.D. of triplicates (***P < 0.001 for the differences in FGFR1 expression between the Ctrl and OSI groups and BMI1 expression between the Ctrl and OSI groups; ns represents non-significant differences in FGFR1 expression between the Ctrl and OSI + SMK-010 groups; **P < 0.01 for the differences in BMI1 expression between the Ctrl and OSI + SMK-010 groups as determined by an unpaired t-test). (C) Venn diagram analysis of common differentially expressed genes (DEGs) upon silencing BMI1 or FGFR1 (|log 2FC| ≥ 1, P < 0.05). (D) KEGG pathway enrichment analysis of DEGs upon silencing BMI1. (E) KEGG pathway enrichment analysis of DEGs upon silencing FGFR1. (F) KEGG pathway enrichment analysis of common DEGs upon silencing BMI1 or FGFR1. (G) Heatmap analysis of differential gene expression changes related to homologous recombination (HR) signaling pathways. (H) RT-qPCR analysis of mRNA levels in 5 representative genes of the HR signaling pathway upon silencing BMI1 or FGFR1. The bars represent the mean ± S.D. of triplicates (****P < 0.0001, ***P < 0.001, and *P < 0.05 for the differences between the siCtrl and siBMI1 or siFGFR1 groups as determined by ANOVA with Tukey's honestly significant difference test for multiple comparisons). (I) HR assay analysis of DSB repair upon SMK-010, OSI alone, or the combination. The bars represent the mean ± S.D. of triplicates (****P < 0.0001 for the differences between the Ctrl and SMK-010 groups; *P < 0.05 for the differences between the Ctrl and OSI groups and OSI and OSI + SMK-010 groups as determined by an unpaired t-test). (J) IF analysis of p-H_2AX upon SMK-010, OSI alone, or the combination (scale bar, 10 μm).

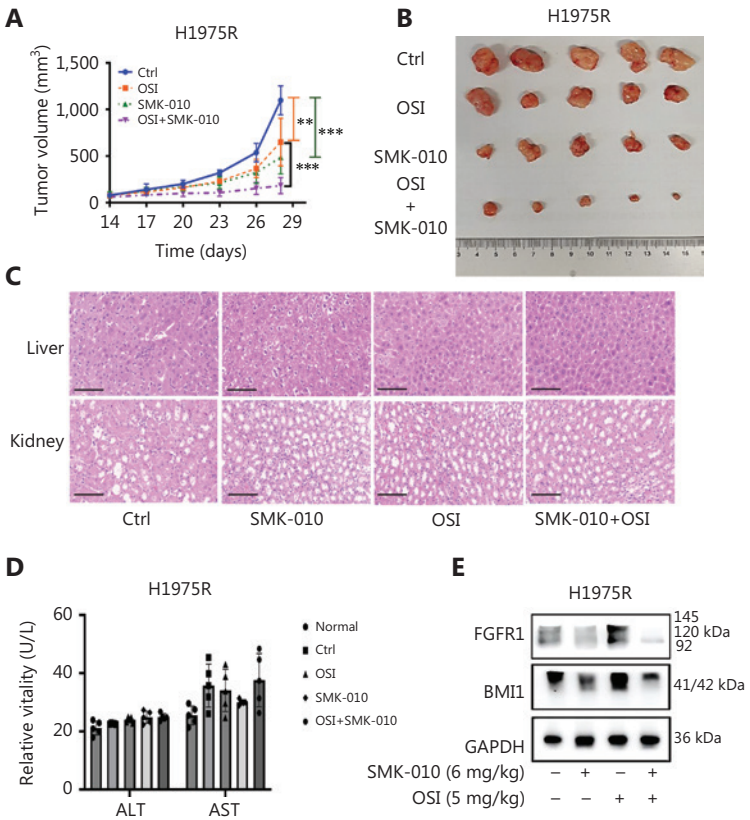

Figure 7 SMK-010 treatment effectually impedes OSI resistance *in vivo*. (A) Quantification of tumor volume on the indicated days after the mice were treated with vehicle, OSI, SMK-010, or the combination (n = 5). The bars represent the mean ± S.D. (**P < 0.01 for the differences between the Ctrl and OSI groups; ***P < 0.001 between the Ctrl and SMK-010 groups and OSI and OSI + SMK-010 groups as determined by ANOVA with Tukey's honestly significant difference test for multiple comparisons). (B) Images of tumors in the H1975R cell subcutaneous model. (C) H&E staining of livers and kidneys of mice (scale bar, 100 μm). (D) ALT and AST kit analysis of liver function in mice. The bars represent the mean ± S.D. of triplicates. (E) Western blot analysis of FGFR1 and BMI1 expression in tumor tissues of mice.

together, these results provided evidence that overexpression of BMI1 may serve as a potential biomarker of a poor prognosis and the development of OSI resistance.

FGFR1 expression was investigated. As shown in **Figure 8H**, FGFR1 was highly expressed in cancer tissues from 3 patients (14.3%) compared to adjacent tissues. Surprisingly, BMI1 was also highly expressed in these cancer tissues. FGFR1 levels were elevated in 6 of the resistant patients [6/16 (37.5%)], decreased in a minor portion of the resistant patients [2/16 (12.5%)], and remained unchanged in the remaining resistant patients [8/16 (50%); **Figure 8I**] compared to the corresponding baseline counterpart tissues. Interestingly, among the 6 OSI-resistant tissues highly expressing FGFR1, 4 also highly expressed BMI1. **Figure 8J** shows IHC images of three representative OSI-resistant lung tissue specimens stained with FGFR1 before and after treatment. Kaplan–Meier survival analysis revealed that high FGFR1 expression was correlated with shorter overall survival in NSCLC patients (**Figure 8K**).

In summary, high levels of BMI1 and FGFR1 expression are closely associated with resistance to OSI, offering guidance for future precision strategies for overcoming such resistance.

Discussion

OSI has emerged as the standard therapy for advanced EGFR-mutated NSCLC. However, the development of resistance severely limits the clinical benefit. While several studies have explored the molecular mechanisms underlying OSI resistance, the resistance mechanisms in approximately 50% of patients remain elusive[35,36]. In this study a novel role for BMI1 in OSI resistance was shown. Compelling evidence was provided indicating that BMI1 regulates FGFR1 and stabilizes FGFR1 by

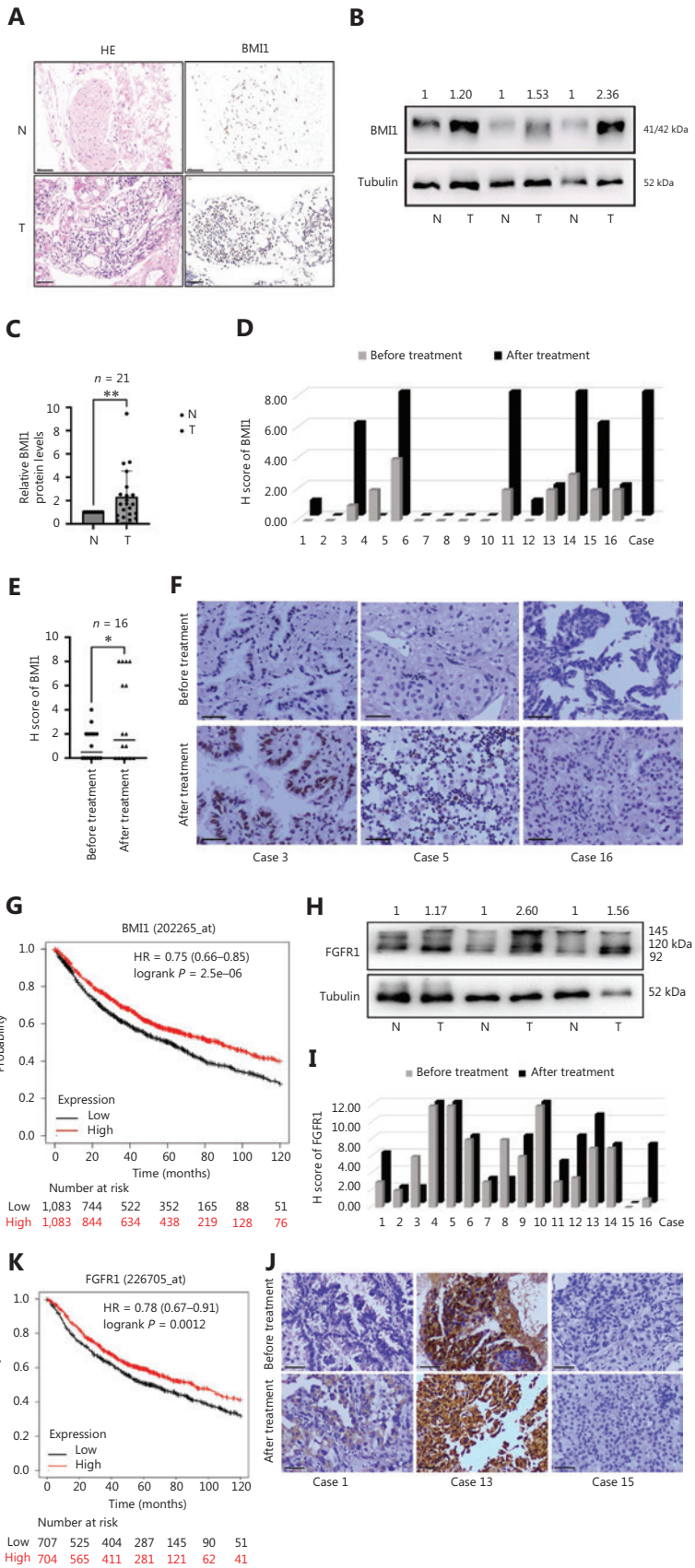

Figure 8 Continued

Figure 8 BMI1 expression positively correlated with poor prognosis and OSI resistance in patient tissues. (A) Hematoxylin and eosin (H&E) staining and immunohistochemistry (IHC) analysis of BMI1 expression in the cancer and adjacent tissues of NSCLC patients (scale bar, 50 μm). (B) Western blot analysis of BMI1 expression in cancer and adjacent tissues of patients with NSCLC. (C) Quantitative analysis of BMI1 expression (n = 21). The bars represent the mean ± S.D. of triplicates (**P < 0.01 for the differences in BMI1 expression between the T and N groups by an unpaired t-test). (D) IHC and H score analysis of BMI1 expression in cancer tissues before and after OSI resistance in 16 NSCLC patients. (E) Quantitative analysis of BMI1 expression (n = 16). The bars represent the mean ± S.D. of triplicates (*P < 0.05 for the differences in BMI1 expression between the after and before treatment groups by an unpaired t-test). (F) IHC images of three pairs of representative OSI-resistant patient lung tissues stained with BMI1 before and after treatment (scale bar, 100 μm). (G) The correlation between BMI1 expression and survival in patients with NSCLC from Kaplan-Meier Plotter was analyzed. (H) Western blot analysis showed that FGFR1 expression was increased in 3 of 21 patients with NSCLC. (I) IHC and H score analysis of FGFR1 expression in cancer tissues before and after OSI resistance in 16 NSCLC patients. (J) IHC images of three pairs of representative OSI-resistant patient lung tissues stained with FGFR1 before and after treatment (scale bar, 100 μm). (K) The correlation between FGFR1 expression and survival in patients with NSCLC from Kaplan-Meier Plotter was analyzed.

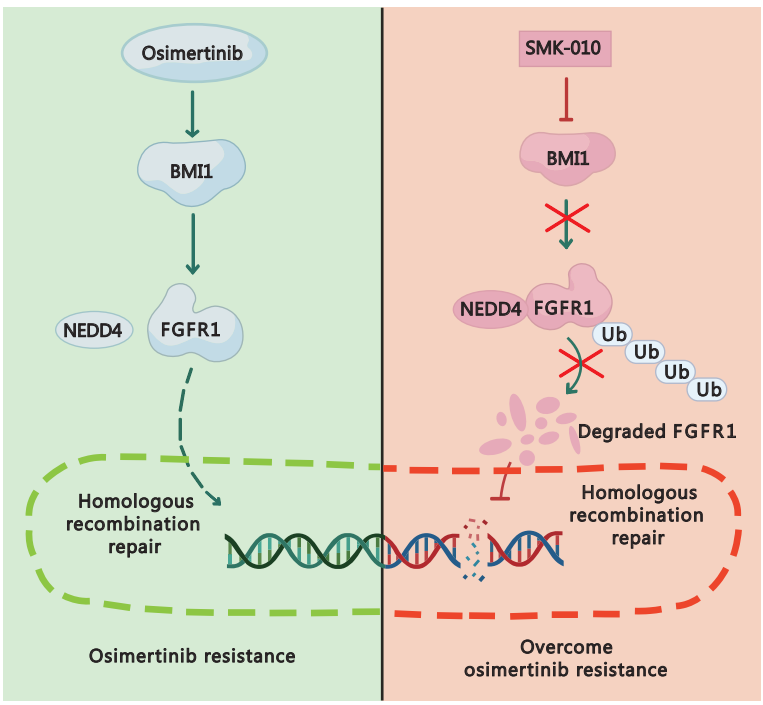

Figure 9 A schematic illustration of the proposed mechanism through which SMK-010 overcomes osimertinib resistance in NSCLC cells. Osimertinib treatment induces expression of B-cell-specific Moloney murine leukemia virus insertion site 1 (BMI1). The high expression of BMI1 can stabilize and activate fibroblast growth factor receptor 1 (FGFR1) by competitively binding to FGFR1 with NEDD4. Subsequently, activated FGFR1 translocates into the nucleus, promoting homologous recombination (HR), which contributes to increased osimertinib resistance. The novel biguanide-derivative, SMK-010, inhibits BMI1 and enhances NEDD4-mediated ubiquitination and degradation of FGFR1 in lysosomes, thereby reducing FGFR1 nuclear translocation. Consequently, combination of SMK-010 and osimertinib mitigates osimertinib-induced activation of the BMI1/FGFR1 axis and HR and ultimately reverses osimertinib resistance.

inhibiting NEDD4-mediated ubiquitination. OSI treatment elevated BMI1 and FGFR1 protein levels and enhanced nuclear co-localization, contributing to OSI resistance in NSCLC. Importantly, silencing BMI1 or the BMI1 downstream protein, FGFR1, reversed this resistance. Furthermore, elevated BMI1 and FGFR1 levels in OSI-resistant cells and paired clinical specimens suggested that the BMI1/FGFR1 axis may serve as a potential biomarker for OSI resistance in NSCLC.

BMI1, a core component of polycomb repressive complex 1, is crucial for maintaining cell self-renewal and proliferation[37,38]. BMI1 is overexpressed in NSCLC and inhibiting BMI1 reverses lung cancer[39]. BMI1 functions primarily as a

transcriptional repressor[40-42]. However, contrary to previous findings, the current study revealed that BMI1 does not regulate FGFR1 at the transcriptional level. Instead, BMI1 was shown to stabilize FGFR1 by preventing NEDD4-mediated proteasomal degradation. FGFR1, a prototypical receptor tyrosine kinase, has been implicated in EGFR-TKI resistance with prior studies focusing on downstream signaling pathways. For example, FGFR1 activates the AKT/mTOR pathway to induce resistance to gefitinib[43]. OSI had a limited effect on p-AKT and upregulated p-ERK1/2 in resistant cells, implying FGFR1 bypass activation. However, factors modulating FGFR1 have rarely been explored. In this study a specific interaction was noted between BMI1 and FGFR1 and BMI1 was shown to regulate FGFR1 post-translation, providing new perspectives on the BMI1/FGFR1 axis in OSI resistance.

Understanding resistance mechanisms is critical for developing advanced therapies to overcome OSI resistance. In this study siRNA technology was used to target BMI1 or FGFR1, which restored NSCLC cell sensitivity to OSI. Moreover, combining BMI1- or FGFR1-specific inhibitors with OSI demonstrated significant synergy. Our laboratory has been dedicated to developing novel biguanide drugs to combat OSI resistance using intermediate derivatization methods[22]. A novel biguanide, SMK-010, was identified through screening which synergized with OSI in *in vitro* and *in vivo* models. Proteomic analysis revealed that SMK-010 significantly decreased FGFR1. Interestingly, further studies revealed that SMK-010 inhibits BMI1 and accelerates FGFR1 lysosomal degradation. Silencing BMI1 or SMK-010 treatment resulted in distinctive FGFR1 degradation pathways. These findings suggested that developing degraders that induce ubiquitylation-mediated FGFR1 degradation may be a breakthrough in improving the efficacy and safety of FGFR1-targeted therapies.

The mechanisms underlying BMI1 or FGFR1 depletion were studied despite the inhibitory effects of SMK-010 on phosphorylation of AKT and ERK1/2, downstream effectors of the FGFR1 signaling pathway. RNA-seq analysis revealed that silencing BMI1 resulted in a greater number of DEGs compared to silencing FGFR1, indicating that BMI1 may regulate additional signaling pathways beyond FGFR1. Notably, HR was enriched among the co-differentiated genes following BMI1 or FGFR1 silencing. HR accurately restores double-strand breaks (DSBs) using intact homologous sequences[44]. Tumor cells with proficient HR have been shown to develop resistance to chemotherapy, radiotherapy, and PARP inhibitors[45,46]. In the present study, OSI was shown to increase HR capacity, while combination treatment with SMK-010 restored HR levels in resistant cells. Additionally, both OSI and SMK-010 alone induced DNA damage and the combination enhanced DNA damage in resistant cells. These results suggested that SMK-010 suppresses HR activity and enhances DNA damage, thereby reversing OSI resistance.

In summary, this study revealed a novel mechanism by which BMI1 regulates FGFR1 to facilitate OSI resistance. Additionally, a new biguanide derivative, SMK-010, has been shown to overcome OSI resistance by inhibiting the BMI1/FGFR1 signaling pathway. Specifically, this is the first study to establish a link between BMI1 expression and OSI resistance in NSCLC. BMI1 stabilized FGFR1 by inhibiting NEDD4-mediated ubiquitination. Importantly, SMK-010 inhibited BMI1, degraded FGFR1, and attenuated OSI-induced increases in BMI1, FGFR1, and HR, thus overcoming OSI resistance (**Figure 9**). This research emphasizes that combining SMK-010 with OSI could be a promising therapy for overcoming resistance to OSI in NSCLC patients. Further clinical investigations are warranted to develop novel therapeutic strategies using SMK-010 to overcome resistance to OSI in EGFR-mutated NSCLC patients. Potential challenges, such as human systemic toxicity and safety profiling, pharmacokinetics and pharmacodynamics, drug delivery, drug-drug interactions, and clinical trial design should be considered for further studies.

Grant support

This work was supported by grants from the National Natural Science Foundation of China (Grant Nos. 82172653 and 82472728), the Key Project of Developmental Biology and Breeding from Hunan Province (Grant No. 2022XKQ0205), the Research Team for Reproduction Health and Translational Medicine of Hunan Normal University (Grant No. 2023JC101), and the Natural Science Foundation of Hunan Province (Grant No. 2025JJ80150).

Conflict of interest statement

No potential conflicts of interest are disclosed.

Author contributions

Conceived and designed the analysis: Mei Peng, Duo Li, Xiaoping Yang.

Collected the data: Mei Peng, Weifan Wang, Di Xiao.
Contributed data or analysis tools: Hui Zou, Xing Feng, Yunhai Yang, Songqing Fan, Xiaoping Yang.
Performed the analysis: Mei Peng, Weifan Wang, Jun Deng.
Wrote the paper: Mei Peng, Xiaoping Yang.

Data availability statement

The data generated in this study are available upon request from the corresponding author.

References

1. Herbst RS, Morgensztern D, Boshoff C. The biology and management of non-small cell lung cancer. Nature. 2018; 553: 446-54.
2. Siegel RL, Miller KD, Wagle NS, Jemal A. Cancer statistics, 2023. CA Cancer J Clin. 2023; 73: 17-48.
3. Lynch TJ, Bell DW, Sordella R, Gurubhagavatula S, Okimoto RA, Brannigan BW, et al. Activating mutations in the epidermal growth factor receptor underlying responsiveness of non-small-cell lung cancer to gefitinib. N Engl J Med. 2004; 350: 2129-39.
4. Paz-Ares L, Tan EH, O'Byrne K, Zhang L, Hirsh V, Boyer M, et al. Afatinib versus gefitinib in patients with EGFR mutation-positive advanced non-small-cell lung cancer: overall survival data from the phase IIb LUX-Lung 7 trial. Ann Oncol. 2017; 28: 270-7.
5. Ramalingam SS, Yang JC, Lee CK, Kurata T, Kim DW, John T, et al. Osimertinib as first-line treatment of EGFR mutation-positive advanced non-small-cell lung cancer. J Clin Oncol. 2018; 36: 841-9.
6. Piper-Vallillo AJ, Sequist LV, Piotrowska Z. Emerging treatment paradigms for EGFR-mutant lung cancers progressing on osimertinib: a review. J Clin Oncol. 2020: JCO1903123.
7. Blaquier JB, Ortiz-Cuaran S, Ricciuti B, Mezquita L, Cardona AF, Recondo G. Tackling osimertinib resistance in EGFR-mutant non-small cell lung cancer. Clin Cancer Res. 2023; 29: 3579-91.
8. Taniguchi H, Yamada T, Wang R, Tanimura K, Adachi Y, Nishiyama A, et al. AXL confers intrinsic resistance to osimertinib and advances the emergence of tolerant cells. Nat Commun. 2019; 10: 259.
9. Leonetti A, Sharma S, Minari R, Perego P, Giovannetti E, Tiseo M. Resistance mechanisms to osimertinib in EGFR-mutated non-small cell lung cancer. Br J Cancer. 2019; 121: 725-37.
10. Yang Z, Yang N, Ou Q, Xiang Y, Jiang T, Wu X, et al. Investigating novel resistance mechanisms to third-generation EGFR tyrosine kinase inhibitor osimertinib in non-small cell lung cancer patients. Clin Cancer Res. 2018; 24: 3097-107.
11. Park HR, Kim TM, Lee Y, Kim S, Park S, Ju YS, et al. Acquired resistance to third-generation EGFR tyrosine kinase inhibitors in patients with de novo $EGFR^{T790M}$-mutant NSCLC. J Thorac Oncol. 2021; 16: 1859-71.
12. Turner N, Grose R. Fibroblast growth factor signalling: from development to cancer. Nat Rev Cancer. 2010; 10: 116-29.
13. Zhou Z, Liu Z, Ou Q, Wu X, Wang X, Shao Y, et al. Targeting FGFR in non-small cell lung cancer: implications from the landscape of clinically actionable aberrations of FGFR kinases. Cancer Biol Med. 2021; 18: 490-501.
14. Terp MG, Jacobsen K, Molina MA, Karachaliou N, Beck HC, Bertran-Alamillo J, et al. Combined FGFR and Akt pathway inhibition abrogates growth of FGFR1 overexpressing EGFR-TKI-resistant NSCLC cells. NPJ Precis Oncol. 2021; 5: 65.
15. Zhang P, Yue L, Leng Q, Chang C, Gan C, Ye T, et al. Targeting FGFR for cancer therapy. J Hematol Oncol. 2024; 17: 39.
16. Peng M, Deng J, Li X. Clinical advances and challenges in targeting FGF/FGFR signaling in lung cancer. Mol Cancer. 2024; 23: 256.
17. Babina IS, Turner NC. Advances and challenges in targeting FGFR signalling in cancer. Nat Rev Cancer. 2017; 17: 318-32.
18. Zhao H, Swanson KD, Zheng B. Therapeutic repurposing of biguanides in cancer. Trends Cancer. 2021; 7: 714-30.
19. Hung MS, Chuang MC, Chen YC, Lee CP, Yang TM, Chen PC, et al. Metformin prolongs survival in type 2 diabetes lung cancer patients with EGFR-TKIs. Integr Cancer Ther. 2019; 18: 1534735419869491.
20. Arrieta O, Barrón F, Padilla MS, Avilés-Salas A, Ramírez-Tirado LA, Arguelles Jiménez MJ, et al. Effect of metformin plus tyrosine kinase inhibitors compared with tyrosine kinase inhibitors alone in patients with epidermal growth factor receptor-mutated lung adenocarcinoma: a phase 2 randomized clinical trial. JAMA Oncol. 2019; 5: e192553.
21. Li L, Jiang L, Wang Y, Zhao Y, Zhang XJ, Wu G, et al. Combination of metformin and gefitinib as first-line therapy for nondiabetic advanced NSCLC patients with EGFR mutations: a randomized, double-blind phase II trial. Clin Cancer Res. 2019; 25: 6967-75.
22. Guan A, Liu C, Yang X, Dekeyser M. Application of the intermediate derivatization approach in agrochemical discovery. Chem Rev. 2014; 114: 7079-107.
23. Bridges HR, Blaza JN, Yin Z, Chung I, Pollak MN, Hirst J. Structural basis of mammalian respiratory complex I inhibition by medicinal biguanides. Science. 2023; 379: 351-7.
24. Xiao D, Lu Z, Wang Z, Zhou S, Cao M, Deng J, et al. Synthesis, biological evaluation and anti-proliferative mechanism of fluorine-containing proguanil derivatives. Bioorg Med Chem. 2020; 28: 115258.
25. Wang L, Fu H, Song L, Wu Z, Yu J, Guo Q, et al. Overcoming AZD9291 resistance and metastasis of NSCLC via ferroptosis and multitarget interference by nanocatalytic sensitizer plus AHP-DRI-12. Small. 2023; 19: e2204133.
26. Xu S, Cao Y, Luo Y, Xiao D, Wang W, Wang Z, et al. Synthesis, anti-proliferative evaluation and mechanism of 4-trifluoro methoxy proguanil derivatives with various carbon chain length. Molecules. 2021; 26: 5775.
27. Wang W, Xiao D, Zhou S, Xu S, Tang X, Zhou X, et al. Synthesis, anticancer activities, and mechanism of N-heptyl-containing biguanide derivatives. Med Chem. 2022; 18: 895-902.

28. Deng J, Peng M, Zhou S, Xiao D, Hu X, Xu S, et al. Metformin targets Clusterin to control lipogenesis and inhibit the growth of bladder cancer cells through SREBP-1c/FASN axis. Signal Transduct Target Ther. 2021; 6: 98.
29. Guo J, Deng N, Xu Y, Li L, Kuang D, Li M, et al. Bmi1 drives the formation and development of intrahepatic cholangiocarcinoma independent of Ink4A/Arf repression. Pharmacol Res. 2021; 164: 105365.
30. van Lohuizen M, Frasch M, Wientjens E, Berns A. Sequence similarity between the mammalian bmi-1 proto-oncogene and the Drosophila regulatory genes Psc and Su(z)2. Nature. 1991; 353: 353-5.
31. Kwon YT, Ciechanover A. The ubiquitin code in the ubiquitin-proteasome system and autophagy. Trends Biochem Sci. 2017; 42: 873-86.
32. Wong A, Lamothe B, Lee A, Schlessinger J, Lax I. FRS2 alpha attenuates FGF receptor signaling by Grb2-mediated recruitment of the ubiquitin ligase Cbl. Proc Natl Acad Sci U S A. 2002; 99: 6684-9.
33. Persaud A, Alberts P, Hayes M, Guettler S, Clarke I, Sicheri F, et al. Nedd4-1 binds and ubiquitylates activated FGFR1 to control its endocytosis and function. EMBO J. 2011; 30: 3259-73.
34. Tang R, Langdon WY, Zhang J. Negative regulation of receptor tyrosine kinases by ubiquitination: key roles of the Cbl family of E3 ubiquitin ligases. Front Endocrinol (Lausanne). 2022; 13: 971162.
35. Fu K, Xie F, Wang F, Fu L. Therapeutic strategies for EGFR-mutated non-small cell lung cancer patients with osimertinib resistance. J Hematol Oncol. 2022; 15: 173.
36. Tang ZH, Lu JJ. Osimertinib resistance in non-small cell lung cancer: mechanisms and therapeutic strategies. Cancer Lett. 2018; 420: 242-6.
37. Rizo A, Olthof S, Han L, Vellenga E, de Haan G, Schuringa JJ. Repression of BMI1 in normal and leukemic human CD34(+) cells impairs self-renewal and induces apoptosis. Blood. 2009; 114: 1498-505.
38. Zheng X, Wang Y, Liu B, Liu C, Liu D, Zhu J, et al. Bmi-1-shRNA inhibits the proliferation of lung adenocarcinoma cells by blocking the G1/S phase through decreasing cyclin D1 and increasing p21/p27 levels. Nucleic Acid Ther. 2014; 24: 210-6.
39. Crunkhorn S. Cancer: BMI1 inhibition reverses lung cancer. Nat Rev Drug Discov. 2016; 15: 678.
40. Yang D, Liu HQ, Yang Z, Fan D, Tang QZ. BMI1 in the heart: novel functions beyond tumorigenesis. EBioMedicine. 2021; 63: 103193.
41. Jia L, Zhang W, Wang CY. BMI1 inhibition eliminates residual cancer stem cells after PD1 blockade and activates antitumor immunity to prevent metastasis and relapse. Cell Stem Cell. 2020; 27: 238-53.e6.
42. Qin K, Lan X, Huang P, Saari MS, Khandros E, Keller CA, et al. Molecular basis of polycomb group protein-mediated fetal hemoglobin repression. Blood. 2023; 141: 2756-70.
43. Zhang D, Han LL, Du F, Liu XM, Li J, Wang HH, et al. FGFR1 induces acquired resistance against gefitinib by activating AKT/mTOR pathway in NSCLC. Onco Targets Ther. 2019; 12: 9809-16.
44. Liu S, Hua Y, Wang J, Li L, Yuan J, Zhang B, et al. RNA polymerase III is required for the repair of DNA double-strand breaks by homologous recombination. Cell. 2021; 184: 1314-29.e10.
45. Groelly FJ, Fawkes M, Dagg RA, Blackford AN, Tarsounas M. Targeting DNA damage response pathways in cancer. Nat Rev Cancer. 2023; 23: 78-94.
46. Huang RX, Zhou PK. DNA damage response signaling pathways and targets for radiotherapy sensitization in cancer. Signal Transduct Target Ther. 2020; 5: 60.

Cite this article as: Peng M, Wang W, Xiao D, Li D, Deng J, Zou H, et al. A novel biguanide-derivative promotes NEDD4-mediated FGFR1 ubiquitination through BMI1 to overcome osimertinib resistance in NSCLC. Cancer Biol Med. 2025; 22: 1381-1404. doi: 10.20892/j.issn.2095-3941.2025.0209